



**HAL**  
open science

## Tree growth stresses, in situ measurement and properties of normal and reaction woods

Bernard Thibaut, Joseph Gril

► **To cite this version:**

Bernard Thibaut, Joseph Gril. Tree growth stresses, in situ measurement and properties of normal and reaction woods. 2020. hal-02984734v1

**HAL Id: hal-02984734**

**<https://hal.science/hal-02984734v1>**

Preprint submitted on 31 Oct 2020 (v1), last revised 8 Jul 2021 (v4)

**HAL** is a multi-disciplinary open access archive for the deposit and dissemination of scientific research documents, whether they are published or not. The documents may come from teaching and research institutions in France or abroad, or from public or private research centers.

L'archive ouverte pluridisciplinaire **HAL**, est destinée au dépôt et à la diffusion de documents scientifiques de niveau recherche, publiés ou non, émanant des établissements d'enseignement et de recherche français ou étrangers, des laboratoires publics ou privés.

1 Title:

# 2 **Tree growth stresses, in situ measurement** 3 **and properties of normal and reaction woods.**

4 Running title: Tree growth stresses

5 Bernard Thibaut <sup>(1), (\*)</sup>

6 Joseph Gril <sup>(2), (3)</sup>

7 <sup>(1)</sup> LMGC, Univ Montpellier, CNRS, Montpellier, France

8 [bernard.thibaut@umontpellier.fr](mailto:bernard.thibaut@umontpellier.fr)

9 <sup>(\*)</sup> Corresponding author

10 <sup>(2)</sup> Université Clermont Auvergne, CNRS, Sigma Clermont, Institut Pascal, Clermont-Ferrand,  
11 France

12 <sup>(3)</sup> Université Clermont Auvergne, INRAE, PIAF, Clermont Ferrand, France

## 13 **Highlight**

14 Experimental study of growth stains on trees restoring their verticality after some accidental  
15 inclination combined to measuring of wood properties at the same position allows to discuss  
16 the functions of forces created by living wood within trees in pre-stressing the woody skeleton  
17 on one side, allowing verticality restoration on the other side.

## 18 **Abstract**

19 Living wood in the tree performs a kind of muscle action generating forces at the sapwood  
20 periphery and thus residual strains in the dead sapwood fibres. Dissymmetric force generation  
21 around tree trunk is a kind of motor system useful for movement, posture control and tree  
22 reshaping after accidents.

23 Rather young trees are able to restore the verticality of their trunk after accidental rotation of  
24 the soil-root system due to wind or some landslide, leading to typical basically curved stems  
25 shape. The very high dissymmetry of forces for the motor action is associated with the  
26 occurrence of reaction wood on one side of the inclined stem during many successive years.

27 A selection of 17 such trees coming from 15 different species (13 different families), tropical  
28 or temperate, hardwoods or softwoods, were selected and peripheral residual strains were  
29 measured in situ before felling, on 8 position for each stem. Associated wooden rods were  
30 sawn and measured for their mechanical and physical properties at green and dry state,  
31 allowing the estimation of tree growth stresses i.e. forces created by the living wood.

32 Thanks to the wide range of wood types, species and basic densities, simple and highly  
33 significant formulas are found for the relationship between green and dry wood properties  
34 such as density, longitudinal modulus of elasticity, specific modulus and two shearing modulus  
35 of elasticity. It was also possible to build easy to use conversion coefficients between growth  
36 stress indicator (*GSI*), measured in situ by the single hole method, and growth strain and  
37 growth stress with the knowledge of basic density and green longitudinal elastic modulus.

38 Growth strains, specific modulus and longitudinal shrinkage are indicators of the fibre wall  
39 properties independent from basic density. Combined to density, they offer a good set of  
40 variables in order to study growth strategy (strains and stresses) and important wood  
41 properties. Compression wood, normal wood and tension wood describe a continuum for  
42 growth strains but do not appear as a continuum for their relationships with the tree  
43 indicators. There should be other basic differences separating these wood types, in the  
44 chemical composition of the matrix and the ultrastructure of cellulose microfibrils.

45 Apart from compression wood, density, specific modulus and longitudinal shrinkage are  
46 largely inefficient for the prediction of growth stresses and a large experimental study is  
47 needed, at first on normal wood only, to investigate chemical determinants of growth stains.

## 48 **Keywords**

49 Force genesis; growth strains; modulus of elasticity; wood shrinkage; tree biomechanics;  
50 wood

## 51 **Abbreviations and notations**

52	MOE, $MOE$	modulus of elasticity in L direction
53	$E_g$	green MOE
54	$E_d$	air-dry MOE
55	$E, E_L$	Longitudinal modulus
56	$G, G_{TL}, G_{RL}$	Shear modulus
57	$\rho$	density
58	$BD$	basic density
59	$DD$	dry density
60	$k$	factor for shear contribution (5/6 for rectangular cross section)
61	SM, $SM$	specific modulus
62	$SM_b$	basic SM
63	$E_L/\rho$	SM in L direction
64	$E_L/G_{TL}, E_L/G_{RL}$	anisotropy factor
65	$GSI$	growth stress indicator
66	$\alpha_m$	maturation strain
67	$\sigma_m$	maturation stress
68	$\phi$	conversion factor $\alpha_m/GSI$
69	$\psi$	conversion factor $\sigma_m/GSI$
70	L, R, T	longitudinal, radial, tangential directions
71	$L_k, R_k, T_k$	dimension in L, R, T direction for condition k
72	$M$	mass

73	$DP_x$	distance to pith
74	$RH$	relative humidity
75	$MC, MC$	wood moisture content
76	$VS, LS$	volumetric, linear shrinkage
77	$FSP$	fibre saturation point
78		

## 79 **Introduction**

80 Tree biomechanics deal with the analysis of mechanical problems encountered by living trees,  
81 including multiphysical couplings between the deformations and movements due to external  
82 forces and the biology of cell formation and growth. A typical case is the classical experiment  
83 of inclining a young tree at the beginning of cambial activity in Spring (Thibaut et al 2001,  
84 Thibaut 2019). In agreement with the physics of viscoelastic materials, the immediate  
85 response is a downward elastic flexure followed by a slow downward creep flexure during the  
86 first 24 hours. But 5 days later the terminal shoot straightens vertically and 3 months later,  
87 apart from a significant growth in length at the apical side, the existing stem shows a change  
88 of curvature (restoration of verticality) opposite to the physical model prediction. The  
89 biological process of wood growth, both in length (primary growth) and in diameter  
90 (secondary growth) should be added to the physical model through appropriate biological  
91 state variables complementing the physical state variables. Based on the functions of living  
92 wood during the three successive phases of cell division, cell wall expansion and cell wall  
93 thickening, three sets of biological variables can be set, in relation to geometrical changes,  
94 mass changes and force generation.

95 Geometrical and mass changes are rather well documented in the literature on tree growth  
96 (Trouvé et al 2015, Fourcaud et al 2008, Deleuze & Houillier 1997, Chave et al 2005). Their  
97 related variables depend on time, genetic growth patterns (architectural model and wood  
98 anatomy) and adaption to environment (climate, tree spacing ...). Forces are needed to  
99 enhance bending strength through pre-stressing (Alméras et al 2018, Gril et al 2017, Thibaut  
100 et al 2001) and to create motor systems (Alméras et al 2005b, Alméras & Clair 2016, Coutand  
101 et al 2007) allowing posture control (vertical or inclined growth) or tree shape restoration  
102 after accidents (apex breaking, rotation of root system ...). They are generated during fibre (or  
103 tracheid) wall thickening (Mellerowicz et al 2001, Plomion et al 2001, Gorshkova et al 2012)  
104 and their level is adapted to the mechanical needs of the tree: high level for slender trees  
105 (Loup et al 2013), with a clear asymmetry between two opposite faces of the wooden axis  
106 when a motor action is needed (Alméras et al 2005b, Moulia et al 2006, Fournier et al 2014).  
107 In the most asymmetrical situation, one side is made of the so-called reaction wood (Gardiner  
108 et al 2014), that differs from normal wood in terms of cell wall ultrastructure and chemical  
109 composition (Côté & Timell 1969, Dadswell & Wardrop 1955, Timell 1986, Yeh et al 2005, Yeh  
110 et al 2006, Ruelle et al 2007, Fagerstedt et al 2014) for the same tree. This is illustrated in  
111 Table 1 for the case of softwoods, with normal wood - comprising opposite wood, lateral wood,  
112 juvenile wood, mature wood or flexure wood - clearly distinct from any type of compression  
113 wood.

114 Table 1 Lignin content for different softwood types

Author	Species	Origin	NW	OW	FW	JW	CW	mCW	sCW	JCW
Brennan et al 2012	Radiata pine		29	27.6	28.7		<b>34.8</b>			
Nanayakkhara et al 2009	Radiata pine	R3+4		27.9				<b>32.9</b>	<b>38.6</b>	
Nanayakkhara et al 2009	Radiata pine	R10		27.3				<b>31.4</b>	<b>35.4</b>	
Nanayakkhara et al 2009	Radiata pine	R15+16		27.1				<b>31.3</b>	<b>35.6</b>	
Nanayakkhara et al 2009	Radiata pine	R1		30			<b>31.6</b>			
Nanayakkhara et al 2009	Radiata pine	R2		27.7			<b>34.9</b>			
Nanayakkhara et al 2009	Radiata pine	Trunk		27			<b>37</b>			
Nanayakkhara et al 2009	Radiata pine	Branch		30.7			<b>39.6</b>			
Funda et al 2020	Scot's pine	Trunk	27.6			27.7				
Yeh et al 2005	Loblolly pine	T. Control	29.4							
Yeh et al 2005	Loblolly pine	T. Windy		28.9			<b>36</b>			
Yeh et al 2005	Loblolly pine	T. Bent		29.1			<b>36.6</b>			
Yeh et al 2006	Loblolly pine	T. Top				29.6				
Yeh et al 2006	Loblolly pine	T. Bottom	27.4			28.5				
Yeh et al 2006	Loblolly pine	T. Middle		28.4		28.6	<b>37.4</b>			<b>37.5</b>
115 Mean			28.4	28.3	28.7	28.6	<b>36.0</b>	<b>31.9</b>	<b>36.5</b>	<b>37.5</b>

116 Rx: ring number from pith; T.: trunk

117 NW: normal wood; OW: opposite wood; FW: flexure wood; JW: juvenile wood

118 CW: compression wood; mCW: mild compression wood; sCW: severe compression wood;

119 JCW juvenile compression wood

120 Bold characters: different lignin content in CW

121 Three parameters can be adjusted during cell wall thickening to fulfil the biomechanical needs  
 122 of the tree: final cell wall thickness, orientation of cellulosic reinforcements, chemical  
 123 composition of cell wall polymers. As a result of this adaptation, variations of physical and  
 124 mechanical properties can be observed in the wood produced by the tree. In this project, trees  
 125 from various species and exhibiting active biomechanical movements were selected.  
 126 Laboratory tests on standard wood specimens sawn from the felled log were related to in-situ  
 127 residual strain measurements that characterize the biomechanical action of the formed wood,  
 128 covering as large a range of situations as possible.

## 129 Material and methods

### 130 *Selection of standing trees*

131 Biomechanical studies (Yoshida et al 2000, Jourez et al 2001b, Thibaut et al 2001, Coutand et  
 132 al 2007, Gril et al 2017) proved that young trees artificially inclined at angles above 20° restore  
 133 progressively their verticality through the production of reaction wood (RW), either tension  
 134 wood (TW) on the top or compression wood (CW) on the bottom of the inclined stem. Wood  
 135 produced on other sides of the stem after inclination, either laterally or opposite, has quite  
 136 similar features both for anatomy and chemical composition. While restoring verticality, the  
 137 trees share a common type of bottom geometry with a basal curvature (Clair et al 2006). In  
 138 natural conditions, accidental inclination of the whole tree by root system rotation due to  
 139 strong wind or landslide can be observed, mostly for young trees. When these trees restore  
 140 verticality in the following years they share the same type of bottom geometry (Fig. 1). They

141 can be considered as natural experiments, and all trees were firstly selected based on this  
 142 criterion.

143 To observe a wide diversity of situations, eleven trees were first selected in a tropical rain  
 144 forest of French Guiana with the help of the botanical expert M.F. Prévost, each from a  
 145 different family - one tree per species and one species per family. Three poplar trees and three  
 146 conifer trees (spruce and pines) from temperate forest in France and China were added to the  
 147 sampling in order to widen the selection (Table 2). For the spruce tree, two logs corresponding  
 148 to two *GSI* measurement levels (see below) were used, at 1m distance from each other. The  
 149 mean diameter at breast height of these 17 trees was 26.5 cm.

150 Table 2 List of trees used in the study

Code	Family	Genus	Species	DBH	RW
1	Melastomataceae	Miconia	fragilis	23.6	GL
2	Meliaceae	Carapa	procera	23.4	GL.
3	Lecythydaceae	Eschweilera	decolorens	23.8	LGL
5	Vochysiaceae	Qualea	rosea	30.3	LGL
7	Cecropiaceae	Cecropia	sciadophylla	25.3	GL
8	Lauraceae	Ocotea	guyanensis	30.9	GL.
9	Flacouritaceae	Laetia	procera	29.4	GLc.
11	Bignonaceae	Jacaranda	copaia	21.7	NGL
12	Myristiceae	Virola	surinamensis	20.4	NGL.
14	Cesalpiniaceae	Eperua	falcata	27.9	GL.
15	Simaroubaceae	Simaruba	amara	27.7	NGL.
16	Salicaceae	Populus	hybrid	38.3	GL
17	Salicaceae	Populus	hybrid	34.8	GL
18	Salicaceae	Populus	hybrid	25.4	GL
E1	Pinaceae	Picea	abies	24.9	CW
E3	Pinaceae	Picea	abies	24.9	CW
PM	Pinaceae	Pinus	pinaster	20.1	CW
PS	Pinaceae	Pinus	sylvestris	23.0	CW
	Mean			26.4	

151

152 DBH: diameter at breast height of the trees in cm

152

153 RW, reaction wood type: GL= tension wood (TW) with gelatinous layer, LGL = TW with a lignified G  
 154 layer, GLc= TW with a multilayer G layer, NGL= TW with no G layer, CW= compression wood

155 *In situ measurements of maturation strain*

156 According to elastic models of residual strain field inside the trunk (Fournier et al 1994a,  
 157 Fournier et al 1994b), the peripheral longitudinal strain locked in recently formed wood is  
 158 directly associated to the maturation force just before fibre death (Thibaut 2019). This  
 159 “maturation strain”  $\alpha_m$  is related to the “maturation stress”  $\sigma_m$  by Hooke’s law  $\sigma_m = MOE * \alpha_m$ ,  
 160 where *MOE* is the modulus of elasticity (*MOE*) of mature wood in the longitudinal direction.  
 161 Several techniques exist for in situ estimation of maturation strain at periphery (Yoshida &  
 162 Okuyama 2002) Clair et al 2013, Yang et al 2005). Here the CIRAD single-hole method was  
 163 used. Two pins are inserted in the trunk surface in longitudinal alignment at 45mm distance  
 164 (Jullien 2013). This distance is measured with a linear displacement transducer before and  
 165 after drilling a hole of diameter 20mm and depth about 20mm in the middle between the two  
 166 pins. The difference in  $\mu\text{m}$  between after and before drilling is called growth stress indicator

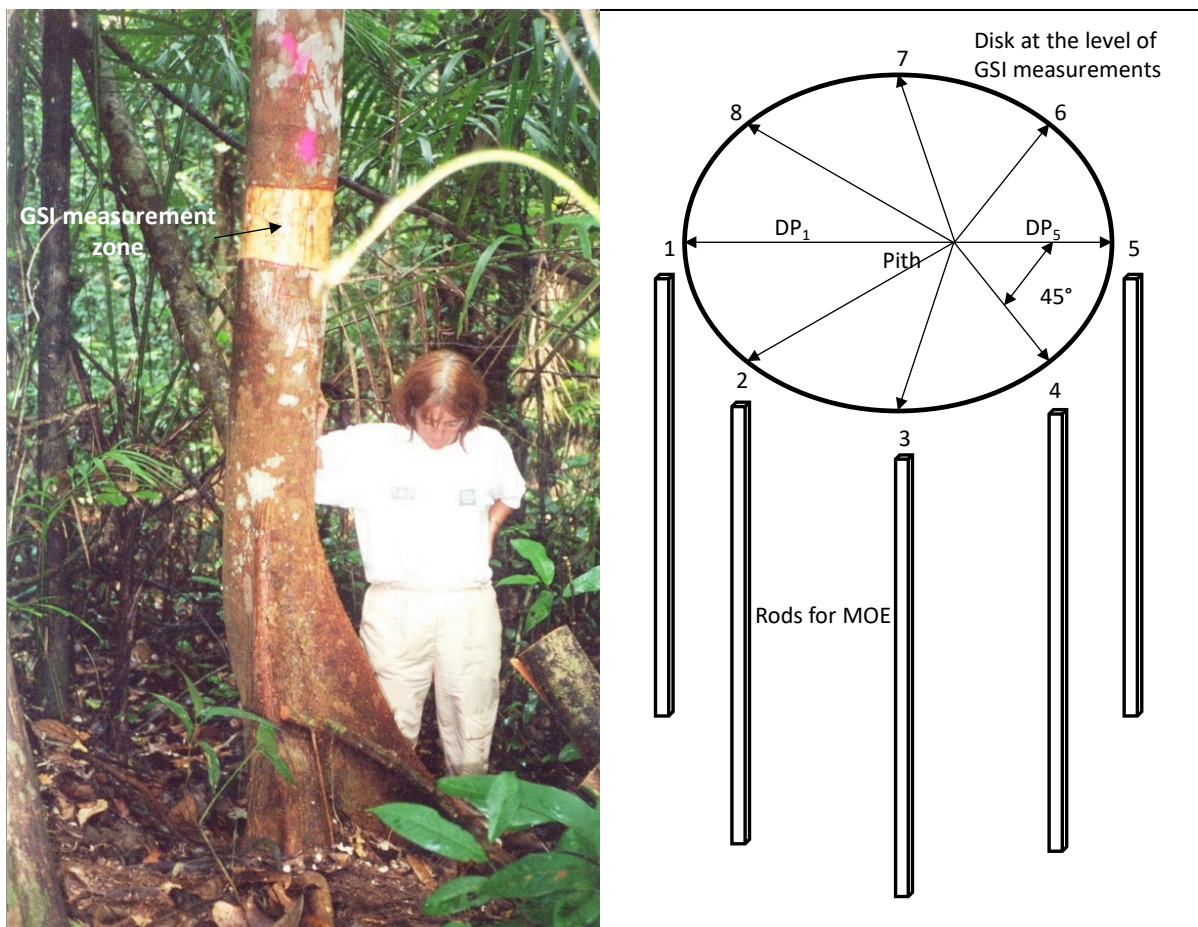
167 (GSI); it is positive for a tension force and negative for a compression force. Eight GSI  
 168 measurements are performed on each tree or tree level, equally spaced around the  
 169 circumference, beginning by the top of the inclined trunk for hardwoods, where tension wood  
 170 is expected, or by the bottom for softwoods, where compression wood is expected.

171 GSI is theoretically (Archer 1984) related to maturation strain  $\alpha$  by the relationship:

172 
$$\alpha_m = \phi * GSI, \alpha \text{ in microstrain } (\mu\epsilon = 10^{-6}), GSI \text{ in } \mu\text{m}, \phi \text{ in } \mu\epsilon/\mu\text{m}$$

173 where the calibration factor  $\phi$  is calculated by modelling the drilling of an anisotropic material  
 174 occupying a half plane, though a complex equation using wood elastic constants and  
 175 geometrical factors (distance between pins and hole diameter), see Annex. For various species  
 176 Baillères (1994) found  $\phi$  values ranging from - 10 to - 15  $\mu\epsilon/\mu\text{m}$ , and Jullien (2013) used - 12.9  
 177  $\mu\epsilon/\mu\text{m}$  for beech.

178 *Wood specimens for physical and mechanical properties measurements.*



179 Fig. 1 Tree measured in French Guiana, wooden disk and rods sawn for each tree  
 180  
 181 DP<sub>x</sub>: distance to pith from the x GSI point

182 Just after cutting each tree, a disk (2cm thick) was crosscut at the level of GSI  
 183 measurements (Fig. 1). Distance from pith to bark (DP<sub>x</sub>) for each GSI measurement position was measured.  
 184 Eight longitudinally oriented rods were sawn just above the disk, at the 8 GSI positions, the  
 185 closest possible to the bark, few days after tree falling, in CIRAD workshop in Kourou.. The  
 186 dimensions of the rods were 500mm (L, longitudinal direction) x 25mm (R, radial direction) x  
 187 25mm (T, tangential direction) and they were kept in green state, wrapped in food-grade

188 transparent cellophane, until the measurement of green MOE ( $E_g$ ). A total of 144 rods were  
189 prepared.

190 A smaller rod (50mm x 25 mm x 25 mm) was cut from these long rods for shrinkage study  
191 after  $E_g$  measurement.

192 The remaining long rods (430mm x 25 mm x 25mm) were air dried in the conditioned chamber  
193 at 65 % air relative humidity (RH) and 20°C temperature until equilibrium, corresponding to  
194 wood moisture content (MC) around 13%. The MOE was again measured on the air-dry rods  
195 as such giving a “crude” air-dry MOE. Rods were then planed on four sides to get standard air-  
196 dry rods (400mm x 20mm x 20mm) and standard air-dry MOE ( $E_d$ ) was measured again.

### 197 *MOE measurements*

198 The flexure free-free vibration method analysed with Timoshenko model (Bordonné 1989,  
199 Brancheriau & Baillères 2002) was used for all measurements. Dimensions in the 3 directions  
200 (L, R, T) and mass ( $M$ ) of the rods was measured with a good precision (0.1%). The rod was put  
201 on 2 thin wires at the first vibration mode positions and tapped at one end, successively on  
202 the radial (TL) and tangential (RL) face, corresponding to the RL and TL hitting plane,  
203 respectively. The resonant frequency  $f_i$  was measured for the three first vibration modes ( $f_1$ ,  
204  $f_2$ ,  $f_3$ ). Using the approximate solution of free vibration theory of Timoshenko, Bordonné  
205 (1989) proved that two useful variables  $x_i$  and  $y_i$  can be built from  $f_i$  frequencies, theoretically  
206 linked by the expression:

$$207 \quad y_i = E/\rho - x_i * E / (k * G)$$

208 where  $E$  is the axial MOE of the rod (the MOE in L direction),  $G$  the shear modulus in the hitting  
209 plane ( $G_{TL}$  or  $G_{RL}$ , depending on the orientation of the rod on the wires),  $\rho$  the rod density and  
210  $k$  a fixed factor. The 3 frequencies ( $f_1$ ,  $f_2$ ,  $f_3$ ) give 3 points of coordinates ( $x_i$ ,  $y_i$ ) allowing to fit  
211 the equation of a straight line with a regression coefficient that should be very close to 1.0.  
212 The slope, the most sensitive to defects, and the intercept of the regression line are  $-E/(k * G)$   
213 and  $E/\rho$ , respectively.  $E/\rho$  is the specific modulus ( $SM$ ) and equals to the square of sound  
214 speed in L direction (unit  $m^2/s^2$ ) while the ratio  $E/G$  ( $E_L/G_{TL}$  or  $E_L/G_{RL}$ ) describes elastic  
215 anisotropy and is useful for the calculation of  $\phi$ . Density is calculated as mass to volume ratio  
216  $\rho = M/(L * R * T)$  and MOE by the formula  $E = SM * \rho$ . Then  $G$  can be derived from  $E$  and  $E/k * G$ ,  
217 with  $k=5/6$  for this geometry (Brancheriau & Baillères 2002).

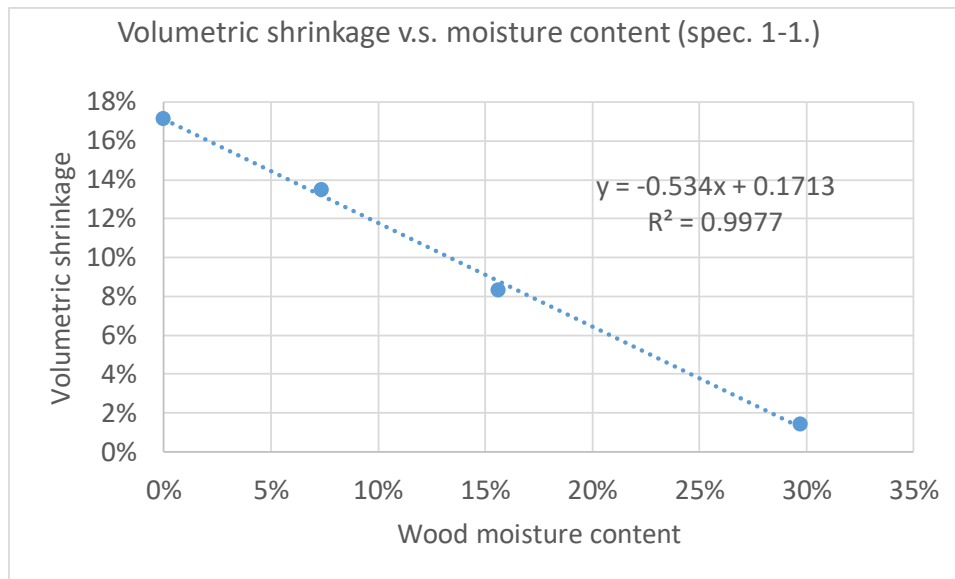
### 218 *Basic density and shrinkage measurements.*

219 Wood density depends on wood moisture content ( $MC$ ). Basic density ( $BD$ ), the ratio between  
220 anhydrous mass and green volume, is a well-defined parameter characterizing wood  
221 honeycomb structure. Wood volume remains constant for green wood until the beginning of  
222 drying, while green moisture content ( $MC_g$ ) can vary widely, typically between 30% and 80%.

223 Shrinkage behaviour of wood (Glass & Zelinka 2010) is necessary to establish relationships  
224 between  $BD$  and dry density at a given moisture content (12% for example). This shrinkage  
225 begins at a reference  $MC$  called fibre saturation point ( $FSP$ ) and is maximum for anhydrous  
226 state ( $MC_0 = 0\%$ ). In order to measure  $FSP$  and shrinkage rate, the small rod ( $L=50\text{mm} \times$   
227  $R=25\text{mm} \times T=25\text{mm}$ ), initially green, is positioned successively in 3 conditioned chambers at  
228 decreasing RH ( $RH = 80\%$ ,  $65\%$ ,  $30\%$ ) and room temperature ( $T=20^\circ\text{C}$ ), then finally in an oven  
229 at  $103^\circ\text{C}$  to obtain the anhydrous state. For each five conditions, mass ( $M_k$ ) and dimensions  
230  $L_k$ ,  $R_k$ ,  $T_k$  are measured. The moisture content is calculated as  $MC_k = (M_k - M_0) / M_0$  where  $k=0$



231 denote the anhydrous state. The volume is derived from the rod dimension using the formula:  
 232  $V_k = L_k * R_k * T_k$ , and volumetric shrinkage ( $VS$ ) at each moisture content is calculated by the  
 233 formula:  $VS_k = (V_g - V_k) / V_g$ . All the points of coordinates ( $MC_k, VS_k$ ) are aligned along a straight  
 234 line of equation  $y = VS - x * VS / FSP$  (Fig. 2) where  $VS$  is the total volumetric shrinkage.



235 Fig. 2 Measurement of volumetric shrinkage and fibre saturation point  
 236

237 Spec. 1-1.: specimen taken at the first *GSI* position for species *Miconia fragilis*

238 The intercepts between this straight line and  $y$  and  $x$  axes are the values of  $VS$  and  $FSP$ ,  
 239 respectively. The total linear shrinkage in direction  $L$  ( $LS$ ) is calculated by the formula:  $LS = (L_g -$   
 240  $L_0) / L_g$ ,  $L_g$  and  $L_0$  being the length of the rod in green and anhydrous state, respectively.

## 241 Results

### 242 Relationships between green and dry properties

243 Because there are more published data on dry than green wood, it is interesting to look at  
 244 relationships between values of useful properties for tree biomechanics (green state) and  
 245 wood mechanics (dry state). Concerning the green state,  $MC_g$  was on average 89%, ranging  
 246 from 38% to 182% (39% to 155% as tree average) and was strongly dependant on wood  
 247 density. The dry state, here, refers to the condition of the specimens after a long storage in a  
 248 room controlled for temperature ( $T = 21^\circ\text{C}$ ) and air relative humidity ( $RH = 65\%$ ). The  
 249 corresponding equilibrium MC ( $MC_d$ ) ranged from 12% to 16% depending on the species and  
 250 wood type within the species.

251 For density, green density depending strongly on the seasonal variations of free water content  
 252 in the xylem,  $BD$  is mostly used instead. The usual proportional relationship, with a very high  
 253 coefficient of determination, was observed between  $BD$  and dry density ( $DD$ ) for this sampling  
 254 (Fig 3). The proportionality coefficient ( $BD/DD$ ) had a mean of 0.826 and ranged from 0.77 to  
 255 0.86. It depended mainly on the total volumetric shrinkage ( $VS$ ) (Fig 4).

256

257  
258

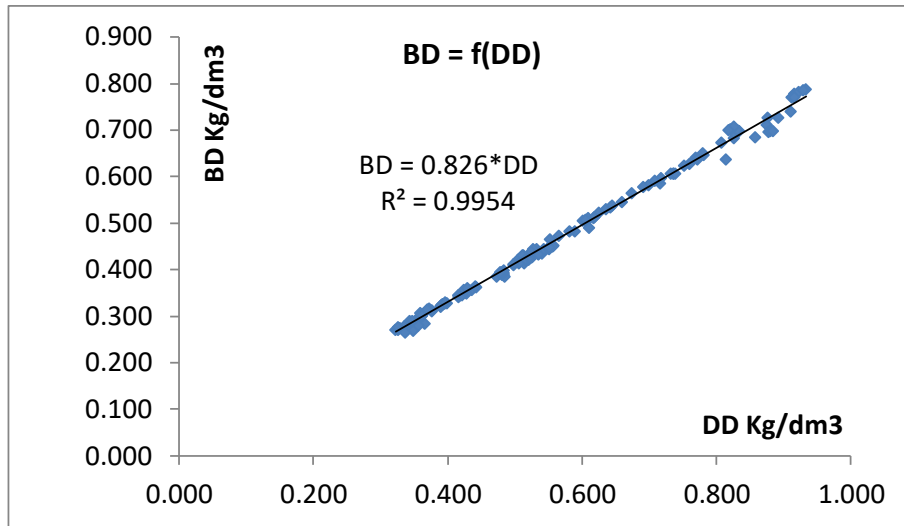


Fig. 3 Proportional relationship between dry and basic density

259  
260

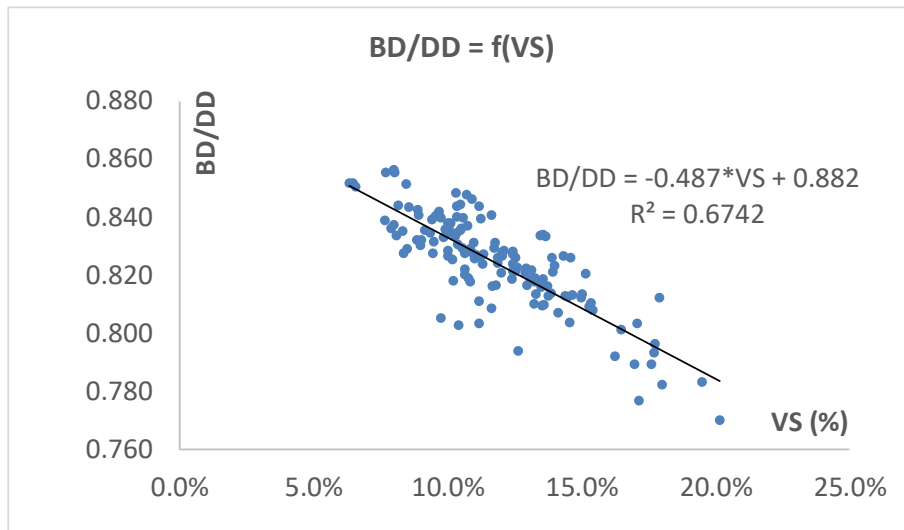
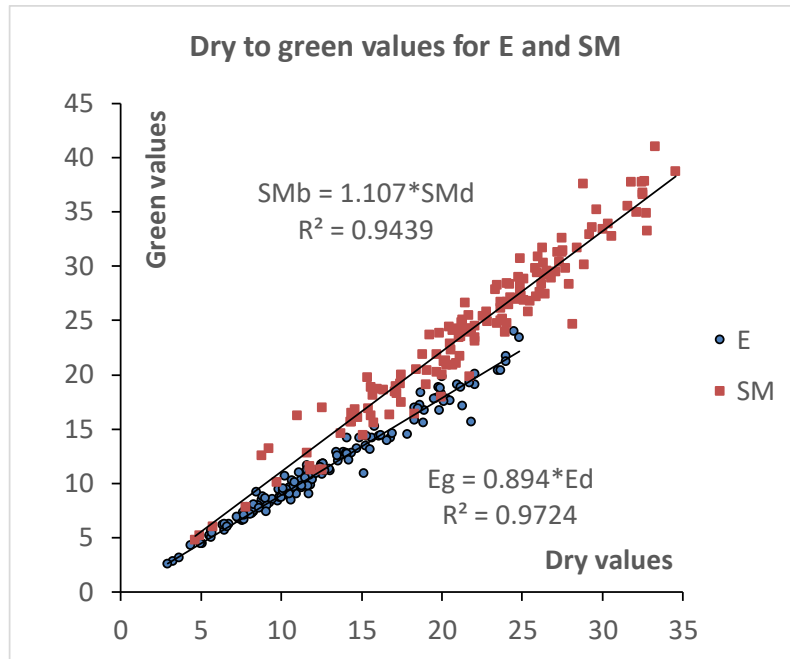


Fig. 4 Dependence of the basic to dry density ratio to the total volumetric shrinkage.

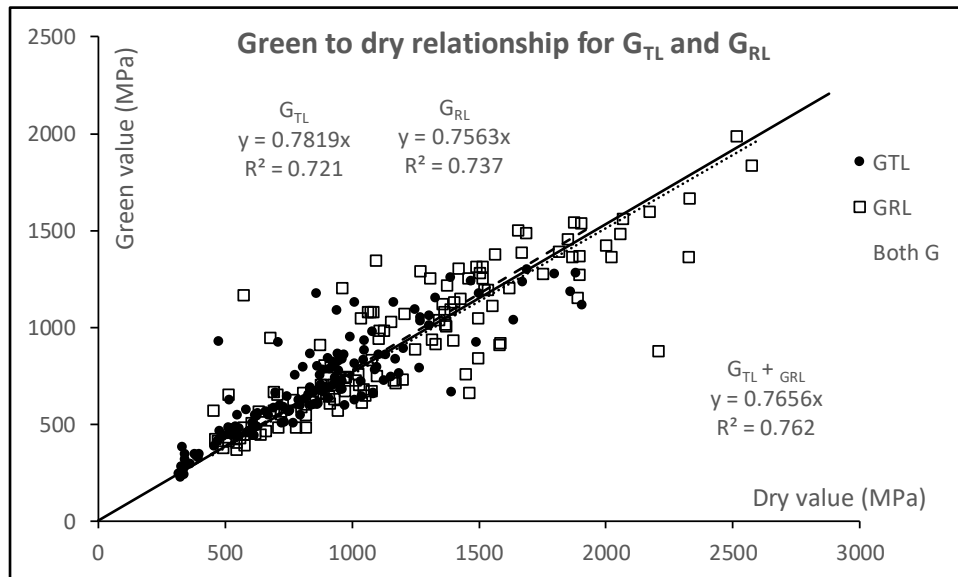
261 For longitudinal elastic modulus ( $E$ ), specific modulus ( $SM$ ) and shear moduli ( $G_{TL}$  and  $G_{RL}$ ),  
262 there is also a proportional relationship between green and dry values. The determination  
263 coefficient ( $R^2$ ) is very high for  $E$  and  $SM$  (Fig. 5) and the influence of MC is relatively small  
264 (around 10% decrease from dry state).



265  
266  
267

Fig. 5 Proportional relationship between dry and green values for longitudinal MOE ( $E$ , MPa) and specific modulus ( $SM$ ,  $Mm^2/s^2$ );  $E_g$ : green MOE;  $E_d$ : dry MOE;  $SM_b$ : basic SM;  $SM_d$ : dry SM.

268 In the case of shear moduli, the proportional relationship is the same for the two directions  
269 (TL and RL) with a lower  $R^2$  mostly due to the much higher sensibility of  $E/G$  (where  $G$  stands  
270 for either  $G_{TL}$  or  $G_{RL}$ ) to small heterogeneities along the rod (Fig 6). MC influence is more  
271 important (around 25% decrease from dry state) but not drastically.



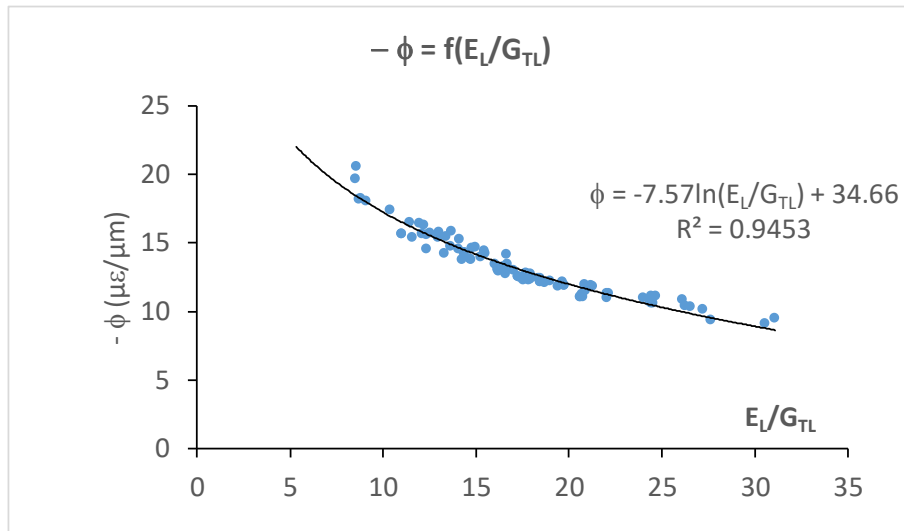
272  
273

Fig. 6 Proportional relationship between dry and green shear moduli

#### 274 *Estimation of maturation strains and stresses*

275 Using the single hole method to estimate residual strains in an orthotropic material requires  
276 the calculation of the conversion parameter  $\phi$  as described in Archer (1984). Baillères in his  
277 PhD thesis (1994) used this calculation for 13 different species. Using elastic orthotropic  
278 constants coming from statistical models built by Guitard and El Amri (1987), he obtained  $\phi$   
279 values ranging from - 9.1 to - 14.9  $\mu\epsilon/\mu m$ . However, special wood types such as RW were not

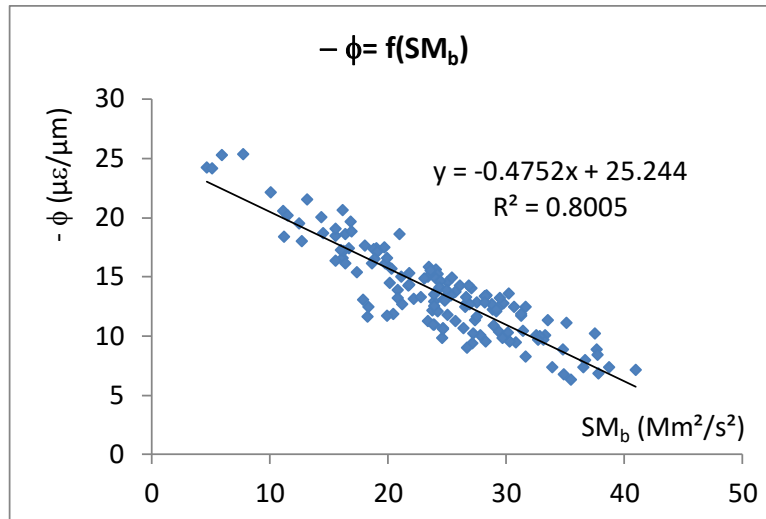
280 considered. Besides, we do not have the 9 elastic constants for the different species and wood  
 281 types (NW and RW) of this study. From Guitard and El Amri and other literature we have built  
 282 a data collection of the 6 diagonal moduli ( $E_L$ ,  $E_T$ ,  $E_R$ ,  $G_{LT}$ ,  $G_{LR}$ ,  $G_{TR}$ ) for different species with  
 283 known densities. We estimated the non-diagonal constants ( $\nu_{LT}$ ,  $\nu_{TL}$ ,  $\nu_{LR}$ ,  $\nu_{RL}$ ,  $\nu_{RT}$ ,  $\nu_{TR}$ ) using  
 284 Guitard's statistical models and then made the whole calculus of  $\phi$  values for these 96 cases  
 285 (Excel sheet in annex 1). In order to make that calculus, we have to find the 2 solutions of a  
 286 second degree equation, which is not possible if the determinant is negative. That happens  
 287 for a few cases (8 with very low  $E/G$  values). There was a very high correlation level between  
 288  $\phi$  and the ratio  $E/G_L$  and a logarithmic equation gives a very high  $R^2$  (Fig.7). This equation:  $-\phi$   
 289  $= -77.57 \cdot \ln(E/G) + 34.665$  can be used to calculate  $\phi$  with only one anisotropic ratio.



290  
 291

Fig. 7 Relationship between conversion coefficient  $\phi$  and anisotropic ratio ( $E/G_{TL}$ ).

292 However, reliable shear moduli data are not always available, so that an alternative method  
 293 to estimate  $\phi$  is needed. Using the previous formula for the 144  $GSI$  measurements, it appears  
 294 that the calculated  $\phi$  was also very well related ( $R^2 = 0.81$ ) to the basic specific modulus ( $SMb$ ),  
 295 the ratio between  $Eg$  and  $BD$  (Fig. 8). The higher dispersion around the regression line can be  
 296 explained by higher uncertainty of  $G$  measurement as compared to  $E$ . Finally, this last formula:  
 297  $-\phi = -0.4811 \cdot SMb + 25.45$ , was used for all specimens. For the very large range of specific  
 298 modulus (from 4.6 to 34.6  $Mm^2/s^2$  for a sampling including RW instead of the usual range  
 299 between 15 to 30  $Mm^2/s^2$  corresponding to NW only) the range of  $\phi$  values is rather large, -  
 300 5.8 to - 23  $\mu\epsilon/\mu m$  instead of - 9.1 to - 14.9  $\mu\epsilon/\mu m$  in Baillères (1994).



301  
302  
303

Fig. 8 Relationship between conversion coefficient  $\phi$  and basic specific modulus. SMb: basic specific modulus (green modulus of elasticity/ basic density) in  $Mm^2/s^2$

304 Maturation stress ( $\sigma_m$ ) is calculated as the product between maturation strain ( $\alpha_m$ ) and green  
305 longitudinal MOE ( $E_g$ ). *GSI* being used for studies on tree reaction (Almérás et al 2005b) or  
306 biomechanical adaptation to forest density (Jullien et al 2013), the relationship between *GSI*  
307 and  $\sigma_m$  was examined at tree level and at population level (our sampling). For each tree there  
308 are 8 pairs of *GSI* -  $\sigma_m$  measurements. For all the trees a proportional relationship was found  
309 with a very high  $R^2$  level (all  $R^2 > 0.97$  and 72% of  $R^2$  values  $> 0.99$ ). This result suggests that it is  
310 perfectly suitable to use *GSI* as a proxy for tree biomechanics at tree level, the conversion  
311 factor  $\psi = \sigma_m / GSI$  (in  $MPa/\mu m$ ) ranging from 0.064 to 0.259 depending on the species (Table  
312 3).

313

Table 3 Mean values of parameters per tree

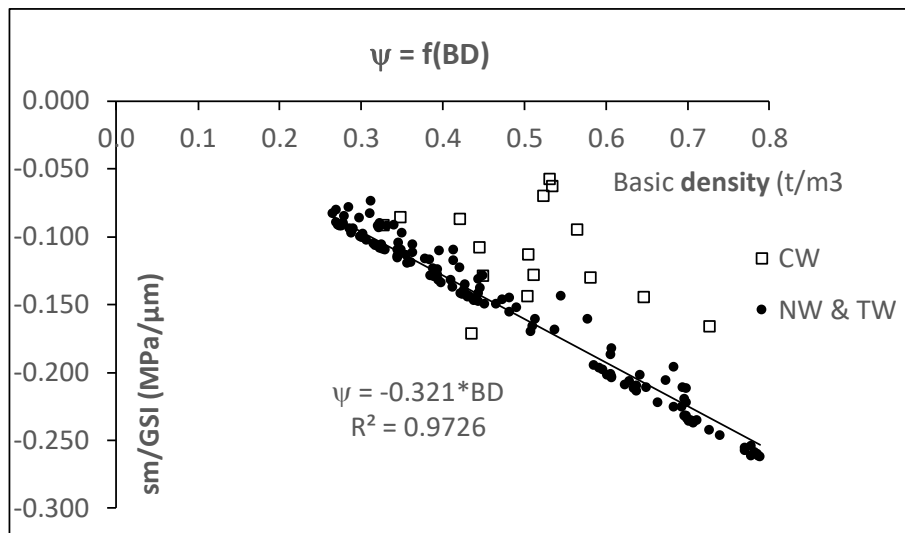
Genus	Species	BD	SMb	Eg	$\psi$	$R^2$
Miconia	fragilis	0.71	26.92	19.0	0.232	0.9997
Carapa	procera	0.61	24.87	15.2	0.203	0.9941
Eschweilera	decolorens	0.78	25.92	20.2	0.259	0.9996
Qualea	rosea	0.56	21.29	12.1	0.199	0.9936
Cecropia	sciadophylla	0.35	34.95	12.3	0.107	0.9788
Ocotea	guyanensis	0.46	27.20	12.7	0.156	0.9903
Laetia	procera	0.66	21.97	14.4	0.218	0.9979
Jacaranda	copaia	0.42	22.14	9.2	0.132	0.9916
Virola	surinamensis	0.29	36.89	10.8	0.084	0.9954
Eperua	falcata	0.70	22.99	16.1	0.234	0.9975
Simaruba	amara	0.30	28.40	8.4	0.096	0.9976
Populus	hybrid	0.29	28.04	8.2	0.110	0.9724
Populus	hybrid	0.34	29.19	9.8	0.114	0.9903
Populus	hybrid	0.38	19.37	7.4	0.128	0.9823
Picea	abies	0.51	20.61	10.0	0.152	0.9933
Picea	abies	0.49	18.10	8.4	0.142	0.9989
Pinus	pinaster	0.42	10.68	11.4	0.064	0.9793
Pinus	sylvestris	0.45	15.88	4.1	0.108	0.9882

314  
315

BD: basic density ( $Kg/dm^3$ ); SMb: basic specific modulus ( $Mm^2/s^2$ ); Eg: green elastic modulus (GPa);

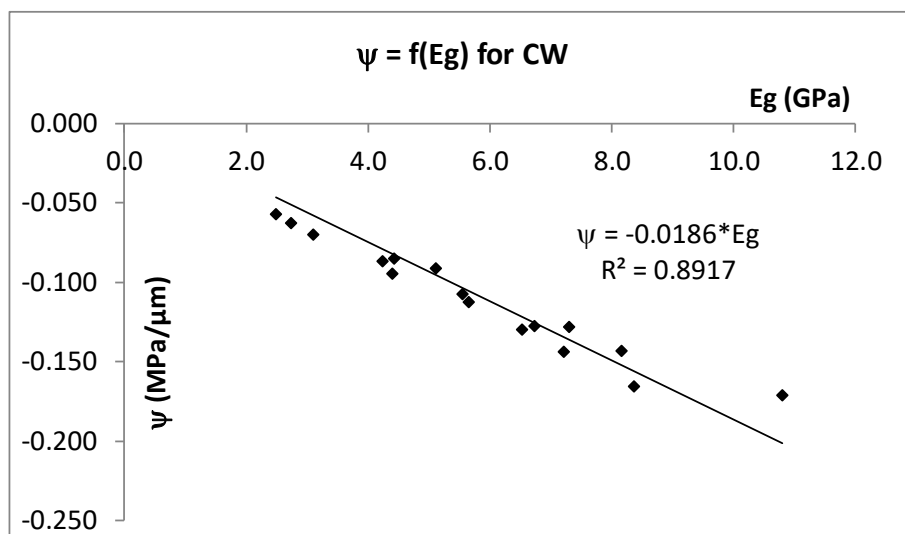
316  $\psi$ : conversion coefficient for maturation stress (in MPa/ $\mu\text{m}$ );  $R^2$  regression coefficient of the  
 317 proportional relationship between  $\sigma_m$  and  $GSI$  within the tree.

318 The global relationship between the conversion coefficient and  $BD$ , for all positions in all trees,  
 319 shows a very good proportional relationship ( $R^2=0.97$ ) when rods containing compression  
 320 wood are excluded (Fig. 9). When no measurement of green elastic modulus is available, basic  
 321 density can be used to calculate the basic specific modulus and then have a good estimation  
 322 of the coefficient factor for maturation strain, this simple formula:  $\sigma_M = -0.321 * BD * GSI$  ( $\sigma_M$  in  
 323 MPa,  $BD$  in  $\text{kg}/\text{dm}^3$  and  $GSI$  in  $\mu\text{m}$ ) can be used for all cases when there is no compression  
 324 wood in the measurement zone.



325  
 326 Fig. 9 Relationship between conversion coefficient for maturation stress ( $\omega$ ) and basic density ( $BD$ ).  
 327  $\psi$ : conversion coefficient for maturation stress (MPa/ $\mu\text{m}$ );  $BD$ : basic density ( $\text{Kg}/\text{dm}^3$ );  
 328  $CW$ : compression wood;  $NW$ : normal wood (hardwood & softwood);  $TW$ : tension wood

329 This is not true for positions with compression wood. A very good proportional relationship  
 330 ( $R^2=0.89$ ) appears between the conversion coefficient and the modulus of elasticity (Fig. 10),  
 331 but when the green elastic modulus is available, together with basic density, it is possible to  
 332 use the conversion coefficient  $\phi$  for maturation strain and then calculate  $\sigma_M$ .



333  
 334 Fig. 10 Relationship between conversion coefficient for maturation stress  
 335 and green modulus of elasticity, for compression wood

336  $\psi$ : conversion coefficient for maturation stress (MPa/ $\mu$ m)  
 337  $E_g$ : longitudinal modulus of elasticity at green state (GPa)

338 *Force generation and longitudinal wood properties*

339 The maturation stress  $\sigma_m$  is the force created by the living wood per unit surface. It is the  
 340 product of the maturation strain ( $\alpha_m$ ) and the green L MOE ( $E_g$ ), itself the product of basic  
 341 density ( $BD$ ) and basic specific modulus ( $SM_b$ ).  $BD$ ,  $SM_b$  and  $\alpha_m$  are the parameters resulting  
 342 from the activity of the living wood until fibre death.

343 A correlation analysis (Table 4) shows that  $\sigma_m$  is mostly dependant on  $\alpha_m$  ( $R^2=88\%$ ) then on  
 344  $SM_b$  (22%) and on  $BD$  (8%). Moreover, the three parameters  $SM_b$ ,  $E_g/G_{TLg}$ ,  $E_g/G_{RLg}$  are very  
 345 strongly correlated. They are all indicators of wood anisotropy. Correlation coefficients  
 346 between  $LS$  and  $\alpha_m$  is weak, although it is known that RWs have strongly different values for  
 347 this property (Jourez et al 2001a, Gardiner et al 2014).

348 Table 4: Correlation (Spearman) coefficients between parameters.

	$\alpha_m$	$\sigma_m$	$BD$	$SM_b$	$LS(\%)$	$E_g$	$G_{TLg}$	$G_{RLg}$	$E_L/G_{TLg}$	$E_L/G_{RLg}$
$\alpha_m$	<b>1</b>	<b>0.941</b>	0.095	<b>0.381</b>	0.196	<b>0.435</b>	-0.049	-0.047	<b>0.431</b>	<b>0.422</b>
$\sigma_m$	***	<b>1</b>	<b>0.290</b>	<b>0.467</b>	0.137	<b>0.685</b>	0.059	0.058	<b>0.559</b>	<b>0.495</b>
$BD$		***	<b>1</b>	<b>-0.346</b>	0.196	<b>0.593</b>	<b>0.790</b>	<b>0.783</b>	-0.094	-0.178
$SM_b$	***	***	***	<b>1</b>	-0.189	<b>0.500</b>	<b>-0.499</b>	<b>-0.508</b>	<b>0.843</b>	<b>0.828</b>
$LS(\%)$	*		*	*	<b>1</b>	-0.074	0.271	0.277	-0.231	-0.175
$E_g$	***	***	***	***		<b>1</b>	<b>0.289</b>	0.255	<b>0.619</b>	<b>0.534</b>
$G_{TLg}$			***	***	**	***	<b>1</b>	<b>0.866</b>	<b>-0.516</b>	<b>-0.473</b>
$G_{RLg}$			***	***	**	**	***	<b>1</b>	<b>-0.421</b>	<b>-0.587</b>
$E_L/G_{TLg}$	***	***		***	**	***	***	***	<b>1</b>	<b>0.877</b>
$E_L/G_{RLg}$	***	***	*	***	*	***	***	***	***	<b>1</b>

349

350 Bold characters: correlation significant at 0.001

351 \*\*\*: correlation significant at 0.001 \*\*: correlation significant at 0.01

352 \*: correlation significant at 0.05

353  $\alpha_m$ : maturation strain in micro-deformation;  $\sigma_m$ : maturation stress in MPa

354  $\phi$  and  $\psi$ : conversion coefficients between  $GSI$  and maturation strain and stress, respectively

355  $BD$ : basic density (anhydrous mass/green volume) in  $kg/dm^3$

356  $LS$ : total longitudinal shrinkage

357  $E_g$ : green longitudinal elastic modulus

358  $G_{TLg}$  and  $G_{RLg}$ : green TL and RL shear modulus, respectively

359  $SM_b$ : basic specific modulus (green longitudinal elastic modulus/basic density) in  $Mm^2/s^2$

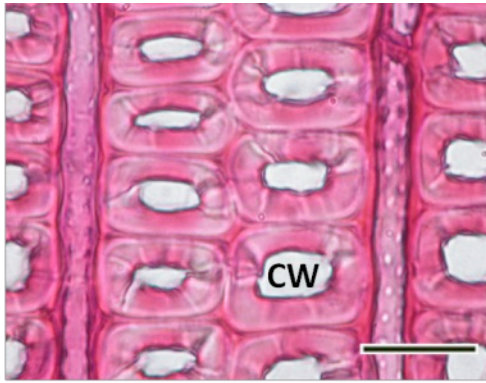
360  $E_g/G_{TLg}$  and  $E_g/G_{RLg}$ : anisotropy ratio in the green state respectively in TL and RL case

361

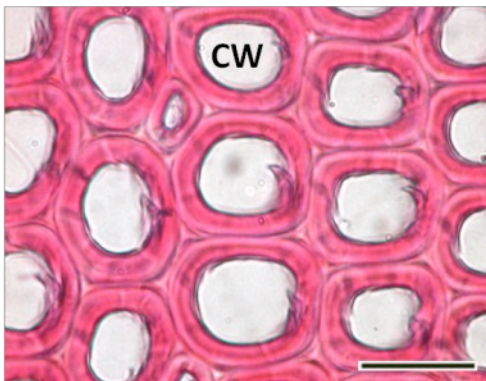
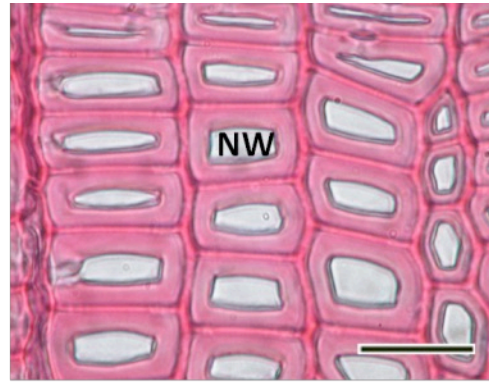
362 Visual observation of the wood disks (Fig 11) allowed affecting a wood type to each tested  
 363 specimen: 1=CW, 2=both CW and NW, 3=NW, 4=both NW and TW, 5=TW. Wood types 2 and  
 364 4 were attributed to rods containing both RW and NW. Transverse sections  $15\mu$ m thick were  
 365 cut from two NW and two TW rods (in the middle of the rod) in order to examine wood  
 366 anatomy (Fig. 12 and Fig.13).



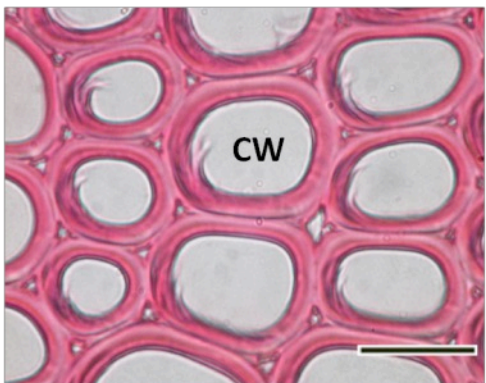
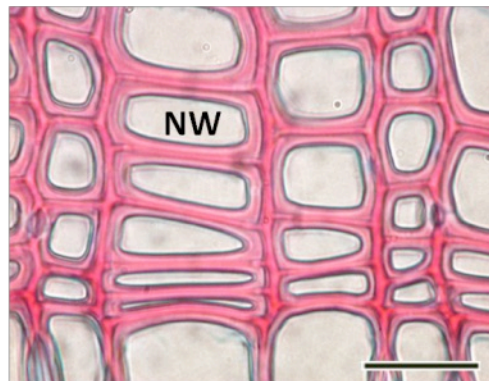




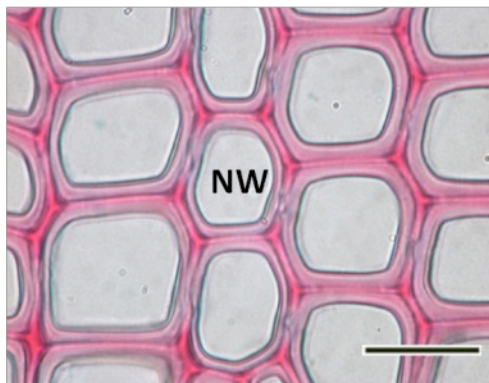
*Picea abies*; Scale bar: 25µm



*Pinus sylvestris*; Scale bar: 25µm



*Pinus pinaster*; Scale bar: 25µm



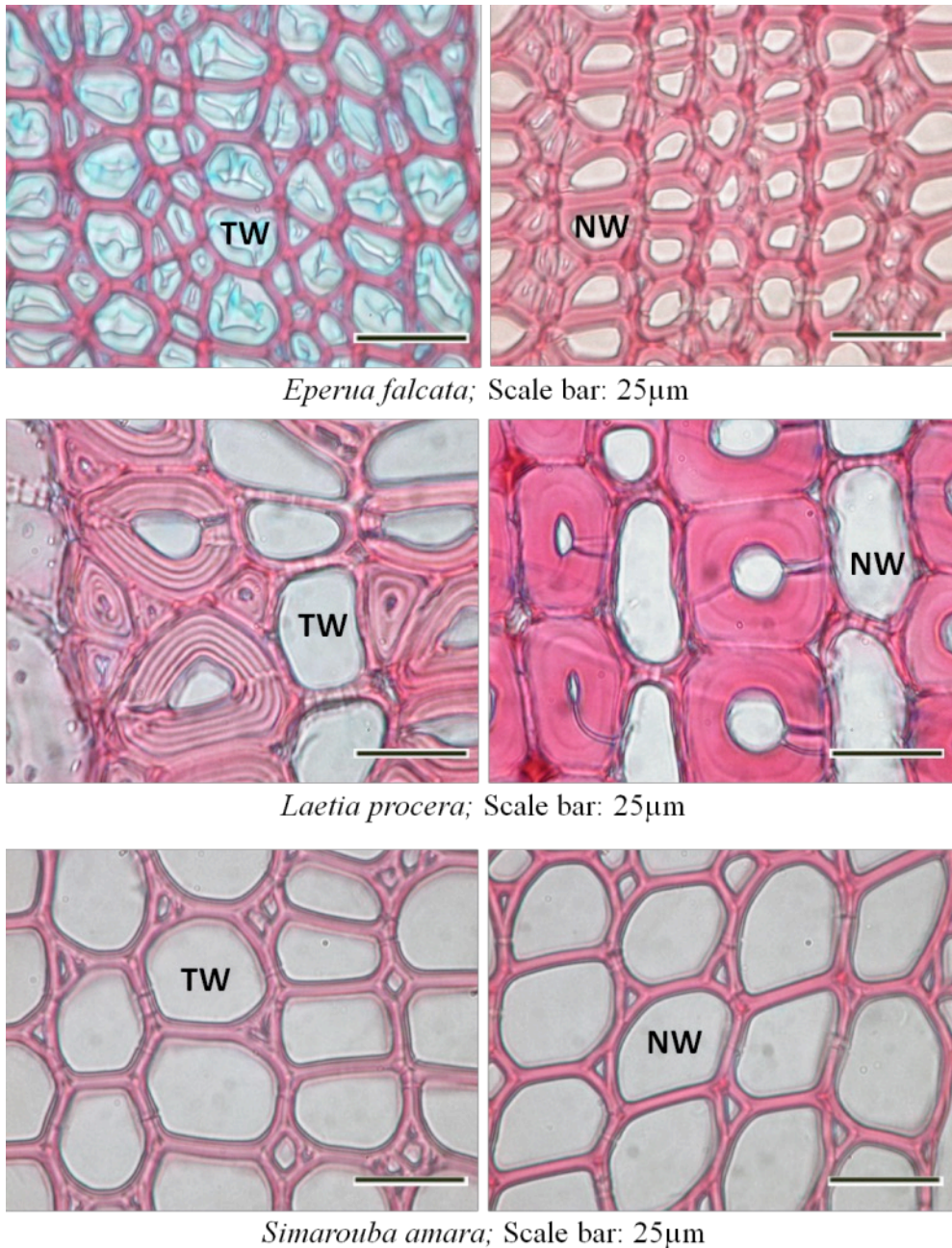
371  
372  
373

Fig. 12 Comparative anatomy of compression wood and normal wood for the conifer species

NW: normal wood; CW: compression wood

374  
375  
376  
377

For conifers, the difference between CW and NW is classical (Ruelle 2014). The mean microfibrillar angle (*MFA*) is always high for CW, and globally lower for NW but with some overlap around 30-35° (Brémaud et al 2013). The trees were rather young (Fig. 11) so most of the NW can be considered as juvenile wood (JW).



378  
379  
380

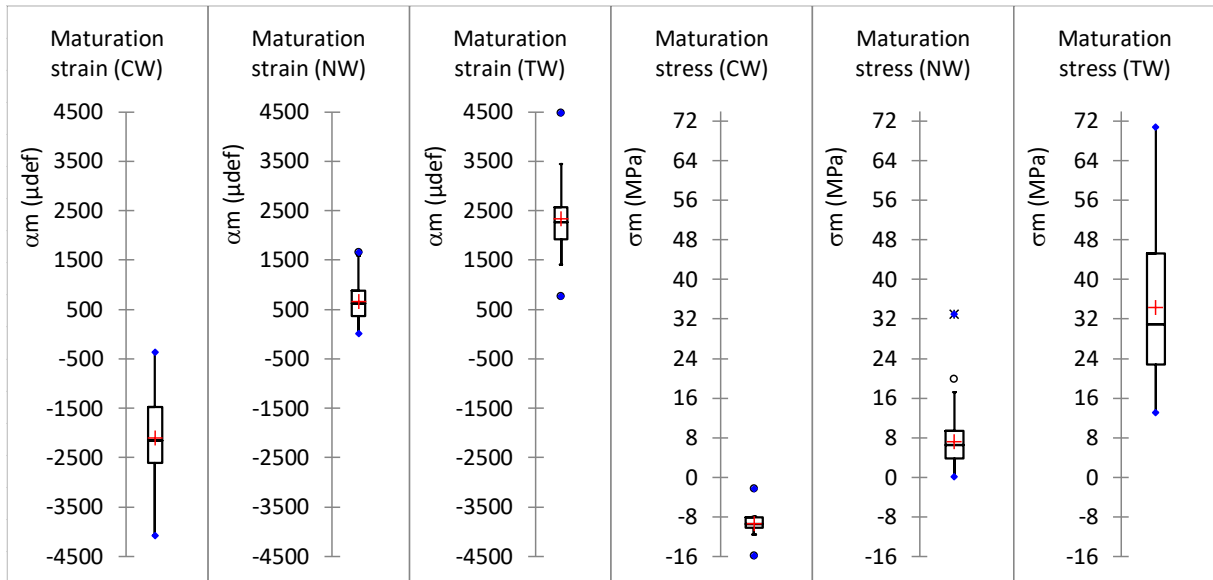
Fig.13 Comparative anatomy of tension wood and normal wood for three tropical species  
NW: normal wood; TW: tension wood

381 For hardwoods, a majority of G-layer type TW (3 poplars, Miconia, Carapa, Ocotea, Cecropia,  
382 Eperua) were studied (Table 2), two species had a lignified G layer (Eschweilera & Qualea),  
383 one a peculiar multi-layered G layer (Laetia) and three no G layer fibre (Jacaranda, Virola,  
384 Simarouba), according to a recent classification based on 242 tropical species (Ghislain et al  
385 2019). Measurement of *MFA* on the 3 species represented in Fig. 13 (Ruelle et al 2007) showed  
386 lower values for TW (2° to 14°) than for NW (10° to 35°), with some overlap around 10°-14° .

387 The clear distinction between wood types for the parameters describing force generation (Fig.  
388 14) results from the very definition of RW as force generator: compression (negative  
389 strain/stress) for CW, slight tension for NW, high tension for TW. Median maturation strain is  
390 very high, around 2200  $\mu$ def (0.22%) in absolute value for both RWs, much lower (620  $\mu$ def  
391 for NW. Median maturation stresses are not so different, in absolute value, between CW (-9.5

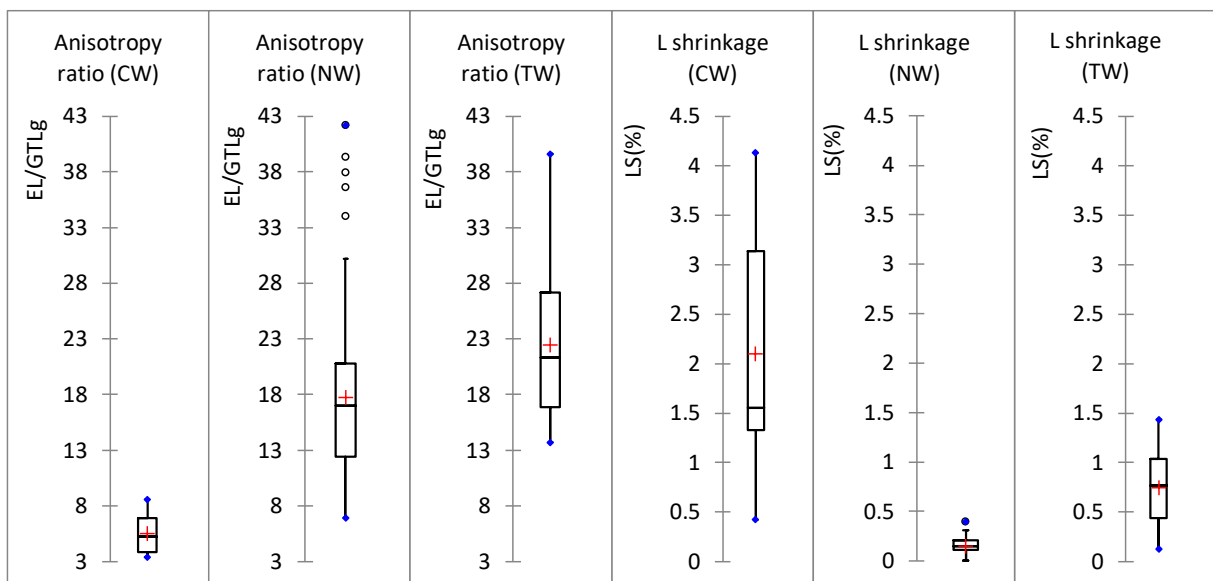
392 MPa, compression) and NW (+6.6 MPa, tension), due to the low value of elastic modulus  
 393 (median 5.5 GPa) for CW (10.2 GPa for NW). The difference increases a little for TW (+31 MPa,  
 394 tension) due to the higher median value of elastic modulus (14.5 GPa), so tensile stress is  
 395 nearly 5 times higher in TW as compared to NW. For a small new ring portion of 100mm<sup>2</sup> (50  
 396 mm wide, 2mm thick) the force created in CW (around 1 kN) or TW (around 3 kN) sectors are  
 397 very high.

398



399 Fig. 14 Distribution of maturation strain and stress values for different wood types  
 400  $\alpha_m$ : maturation strain in micro-deformation;  $\sigma_m$ : maturation stress in MPa  
 401 CW: compression wood; NW: normal wood; TW: tension wood  
 402

403 The parallel regular progression of values for anisotropy factor shown in Fig 15, reflects the  
 404 fact that the *MFA* decreases from CW (up to 50°) to TW (near to 0°), with, however, a large  
 405 overlap between NW and TW and a smaller one between NW and CW. This is not true for *LS*  
 406 (Fig. 15 and Fig. 16): both RWs have a high *LS* while NW keeps a very low *LS* level (less than  
 407 0.4%).



408 Fig. 15 Distribution of L shrinkage (*LS*) and anisotropy ratio (*E/GTLg*) for different wood types  
 409

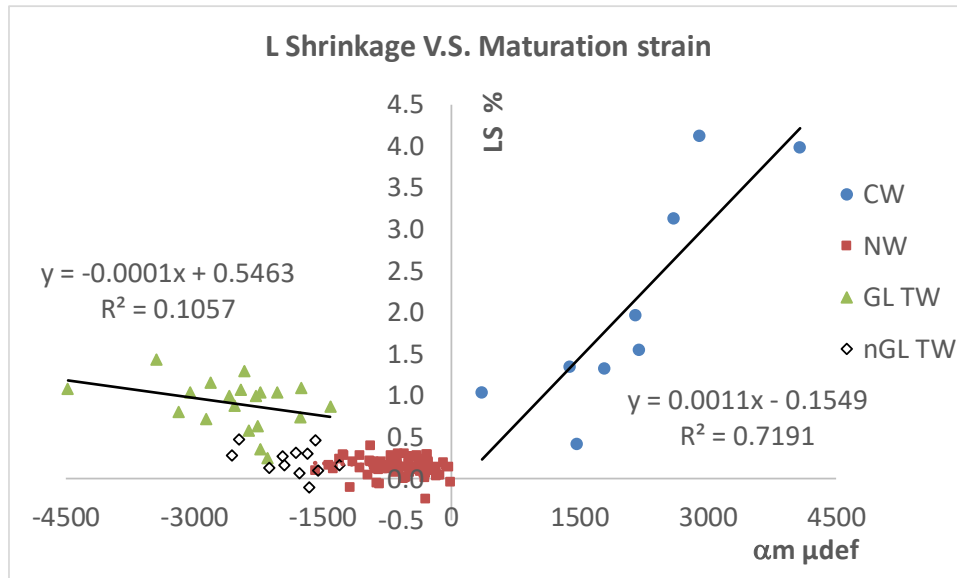


410  
411

$LS$ : longitudinal shrinkage,  $E_g/G_{TLg}$ : anisotropy ratio at green state.  
same legend as Fig. 11

412 The relationship between  $LS$  and  $\alpha_m$  (Fig. 16),  $\alpha_m$  and  $SMB$  (Fig. 17) or  $LS$  and  $SMB$  (Fig. 18)  
413 evidences different patterns for NW, CW and TW. It should be noted that  $\alpha_m$  and green wood  
414 properties ( $LS$  and  $SMB$ ) are not strictly measured on the same material and this contributes  
415 to lower correlations between them.

416  $LS$  grows with the absolute value of  $\alpha_m$  (Fig. 16) for both CW and GL-TW while  $LS$  keeps low  
417 for all the NWS.



418  
419

Fig. 16 Evolution of longitudinal shrinkage with maturation strain

CW: compression wood

NW: normal wood for both softwoods and hardwoods (no significant difference)

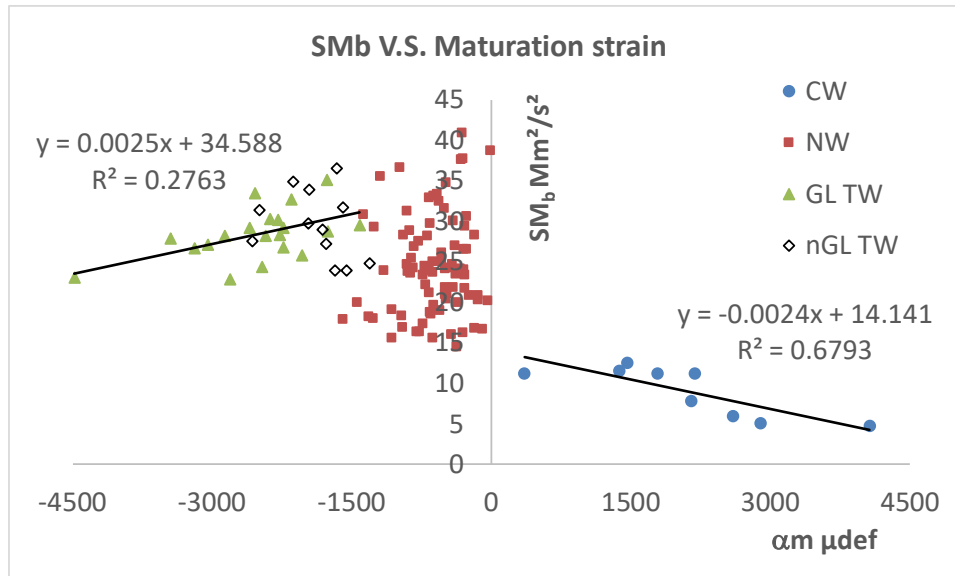
GL-TW: tension wood with gelatinous layer

nGL-TW: tension wood without gelatinous layer

424

$\alpha_m$ : maturation strain;  $\mu\text{def}$ : micro deformation ( $10^{-6}$ )

425 There is no evident influence of  $\alpha_m$  on  $SMB$  (Fig.17) for NW while  $SMB$  increases when  $\alpha_m$   
426 decreases in absolute value for both TW and CW.



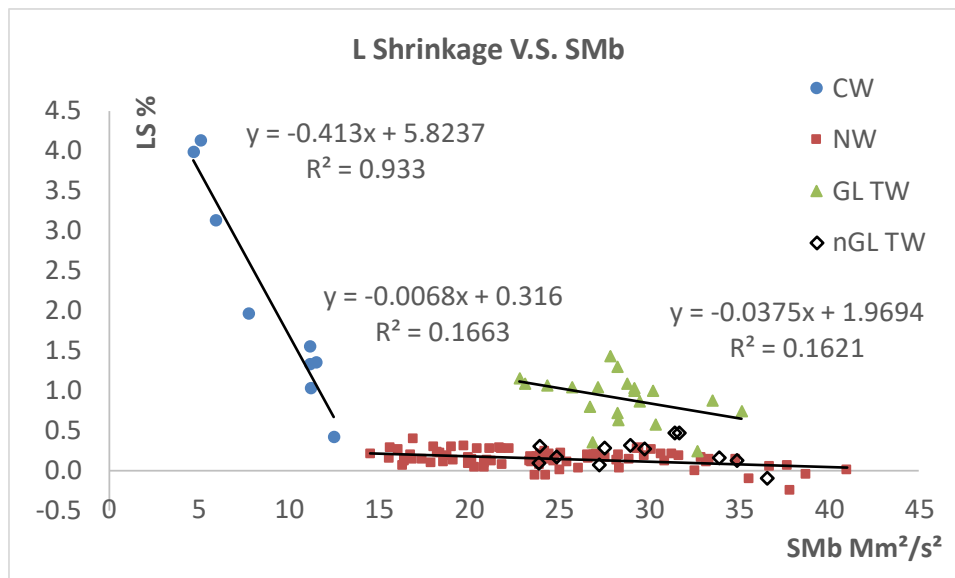
427 Fig. 17 Evolution of longitudinal maturation strain with wood elastic anisotropy

428 Same legend as Fig. 16

429 Smb: basic specific modulus (green modulus/basic density)

430

431 *LS* and *Smb* are measured on the same rod so the uncertainties are lower. For all wood types  
 432 *LS* decreases significantly when *Smb* increases (Fig. 18) but the evolution is rather steep or  
 433 very steep for TW and CW while it is smooth for all NWs. It should be noted that the TW of  
 434 species without G layer is similar to NW for this relationship. High L shrinkage is mostly present  
 435 when there is a G layer in the TW fibre.



436 Fig. 18 Evolution of longitudinal shrinkage with wood elastic anisotropy

437 Same legend as Fig. 16 & 17

438

## 439 Discussion

### 440 *Green to dry wood properties*

441 *BD* is now commonly used in ecological studies on carbon sequestration in forests. Using the  
 442 large CIRAD database (4022 trees) a very nice proportional relationship was found between  
 443 *DD* (12% moisture content) and *BD* with a proportional factor of 0.828 (Vieilledent et al 2018).

444 Here, with a quite different sampling, a factor of 0.826 was obtained. The very large range of  
445 VS due to the presence of CW shows that this proportional factor ranges from 0.78 to 0.86  
446 (Fig. 4) with a good prediction of the variation by VS which can be easily measured at the same  
447 time as BD.

448 In our study, elastic properties are measured by vibration technique, namely high deformation  
449 rate where little viscosity is active (no creep added to the instantaneous elastic strain). The  
450 decrease between dry and green state is only around 10% for  $E$  and around 25% for  $G$ , either  
451  $G_{RL}$  or  $G_{TL}$ . The Wood Handbook (Gretschman 2010) gives MOE values in the green state and  
452 at 12% MC, as means for 64 hardwood species and 37 softwood species, using different rods  
453 for each condition in order to measure also rupture strength. A very good proportional  
454 relationship is also obtained ( $R^2=0.86$  for hardwoods,  $R^2=0.95$  for softwoods), as compared to  
455  $R^2=0.97$  in this study. The decrease between air-dry and green states is around 20% (22% for  
456 hardwoods, 20% for softwoods), which is significantly different (two times greater). A small  
457 part of the difference can be explained by a different equilibrium MC (from 12% to 16% for  
458 air-dry wood in this study), but the greatest part is likely to originate from the experimental  
459 method. In the Wood Handbook the measurements are performed in 3 points bending at slow  
460 deformation rate, allowing some initial creep which is more important for green wood than  
461 for dry wood.

#### 462 *GSI as a good indicator for growth stresses*

463 The single hole method has the advantage of being quick, easily operable in all field situations  
464 and cheap, making it most appropriate for large measurement campaigns such as the  
465 "Stresses in beech" EU project where 8,000 GSI data were collected in situ (Jullien et al 2013).  
466 It requires, however, the use of a conversion factor ( $\phi$ ) from GSI to  $\alpha_m$ . The theoretical  
467 computation of  $\phi$ , based on an orthotropic elastic model of residual stress (Archer 1984),  
468 depends of wood anisotropy near the measurement zone and thus depends on the wood  
469 species as well as the wood type. It can be practically estimated from the basic specific  
470 modulus ( $SM_b$ ) that ranges from 5  $Mm^2/s^2$  for severe compression wood to up to 40  $Mm^2/s^2$   
471 for resonance wood with high sound speed. The range of resulting maturation strains found  
472 in this study is very similar to values in the literature for CW (Yamamoto et al 1991, Huang et  
473 al 2001, Yamashita et al 2007) and TW (Yoshida et al 2000, Fang et al 2008, Clair et al 2013),  
474 around -4000 to +4000  $\mu\text{def}$ .

475 The 8 maturation stresses calculated for each tested tree were proportional to GSI values with  
476 very high regression coefficients ( $R^2>0.97$ ), so it is possible to use GSI as a proxy of growth  
477 stress within a tree, even when it contains severe CW or TW sectors. Furthermore, the  
478 conversion coefficient  $\psi$  between GSI and maturation stress is proportional to BD with a very  
479 good regression coefficient ( $R^2=0.97$ ), except in the case of CW occurrence. This means that  
480 for hardwoods, BD is the only parameter needed for the conversion coefficient  $\psi$ .

#### 481 *Strain, stress and force generation.*

482 Force generation is one of the functions provided by fibres/tracheids during cell-wall  
483 thickening, and force asymmetry between both sides of a wooden axis is the motor of its  
484 posture control (Almérás et al 2005b, Almérás et al 2009). The force ( $F$ ) produced by an  
485 angular portion of new living xylem equals the product of the area ( $A$ ) of that portion,  
486 orthogonal to the force, by the maturation stress ( $\sigma_m$ ) generated in the xylem tissue during  
487 cell-wall thickening:  $F=A \cdot \sigma_m$ .  $A$  depends both on the amount of cell division in the cambium  
488 and on the cell expansion until the end of primary wall setting (Cuny et al 2012).  $\sigma_m$  is also the

489 residual stress present in the last ring of sapwood after the programmed fibre death, and can  
490 be measured in situ by classical residual stress measurement methods. The existence of this  
491 pre-stress enhances the flexure resistance of wooden axes (Gril et al 2017) and thus  
492 contributes to the skeleton function of wood in the tree.

493 Maturation stress  $\sigma_m$  is associated to maturation strain  $\alpha_m$  via Hooke's law:  $\sigma_m = E \cdot \alpha_m$ , where  
494  $E$  stands here for  $E_g$ , the MOE of xylem tissue at the end of the maturation process.  $\alpha_m$  is  
495 locked in the wood until stress release, e.g. by cutting. It is largely agreed that  $\alpha_m$ , as a result  
496 of the whole lignification process, is the source of  $\sigma_m$ . As the new layer is glued on a solid rigid  
497 core, the "natural" extension or shrinkage of the fibre cannot be expressed, resulting in stress  
498 occurrence.

499 This longitudinal expansion during secondary wall deposition is of the order of 0.1%, much  
500 smaller than the expansion occurring during primary wall building. But, at the end of the  
501 maturation process, the MOE of a xylem portion is very high, of the order of 10 GPa, thousands  
502 of times bigger than the modulus at the end of primary wall expansion. As a result, maturation  
503 stresses have high values allowing to produce large forces (of the order of kN) and large motor  
504 actions (Alm eras et al 2005b).

505 In the L direction, thanks to the honeycomb-like microstructure of wood with a quasi-parallel  
506 alignment of the wall of fibres or tracheids, wood MOE ( $E$ ) is directly related to cell-wall MOE  
507 ( $E_w$ ). Below  $FSP$ , when cell cavities (lumens) contain only air and water vapour, wood specific  
508 modulus  $SM=E/d$  equals that of the cell-wall  $SM_w=E_w/d_w$ , where  $d_w$  is the cell-wall density;  
509 both being equal to the square of the longitudinal sound speed (Gibson and Ashby 1999).  
510 Wood MOE can thus be expressed as:  $E = d \times SM = d \times SM_w = (d/d_w) \times E_w$ . In this expression the  
511 relative density ( $d/d_w$ ) represents the cell-wall proportion; it is a basic property of the cellular  
512 material, while  $E_w$  is a basic property of the cell wall. Both  $d_w$  and  $E_w$  depend on the properties  
513 of the polymers composing the cell wall; while  $d_w$  variation is very small among wood species  
514 and types ( $d_w \sim 1.5\text{g/cm}^3$ ),  $E_w$  is highly dependent on the ultrastructural organisation of the  
515 cell wall such as the orientation of cellulosic microfibrils. The longitudinal maturation strain  
516  $\alpha_m$ , like  $E_w$ , depends on cell-wall composition and organization.

517 Wood formation involves three successive processes: cell division, expansion and maturation:  
518 the number of cells produced during a given period of time is controlled by cell division, their  
519 size by cellular expansion and the properties of their wall by cellular maturation (taken here  
520 in a broad sense, including the cell-wall thickening). Wood relative density ( $d/d_w$ ),  
521 approximately proportional to the ratio between cell-wall thickness and cell diameter, is  
522 controlled both by division and by maturation, while cell-wall MOE ( $E_w$ ) and maturation strain  
523 ( $\alpha_m$ ) are mostly controlled by maturation. Wood MOE ( $E$ ), as the product of  $E_w$  and  $d/d_w$ , and  
524 maturation stress  $\sigma_m$ , as the product of  $E$  and  $\alpha_m$ , are both controlled by expansion and  
525 maturation. When a layer of wood is deposited at stem periphery, the force produced by a  
526 portion of that ring, equal to the product of  $\sigma_m$  and the ring thickness, is controlled by  
527 expansion and maturation, and by division - and so is the bending motor force produced at  
528 the stem level, since it amounts, roughly, to the product of the driving forces on the two  
529 opposite faces and the total diameter growth. The regulation of such a scheme is very complex  
530 and is far from being fully understood today. Anyway, this regulation of forces is also, at the  
531 end, a regulation of all wood properties because it affects chemistry, anatomy, and cell-wall  
532 ultrastructure.

533 *Compression wood, normal wood and tension wood*

534 It is natural and useful to use maturation strain  $\alpha_m$  as basic indicator of maturation because it  
 535 depends only on this living phase, but it is also the case of  $E_w$  as well as of longitudinal  
 536 shrinkage ( $LS$ ), which depend essentially only the composition and structure of the cell wall.  
 537 Hence the relationships between these three parameters can provide information on what  
 538 happened during secondary wall thickening until programmed cell death.

539 The distinction between wood types is based on  $\alpha_m$ : CW produces positive  $\alpha_m$ , TW very large  
 540 negative  $\alpha_m$  and NW very low to rather high negative  $\alpha_m$ . All have a muscular action for the  
 541 control of stem curvature: NW alone for a moderate action, or combined with RW (either CW  
 542 or TW) for a strong action. Many papers highlight that triggering RW mobilise specific genes  
 543 (Gardiner et al 2014) and changes strongly the chemical composition of the cell wall matrix as  
 544 compared to NW. This is probably what explains the different patterns in the relationships  
 545 observed in Fig. 15, 16 & 17.

546 For NW, no significant difference seems to exist between softwoods and hardwoods in spite  
 547 of chemical differences in chemical composition of the matrix, mainly for the hemicelluloses  
 548 (Gérard et al 2020). For all NWs there is a wide range of  $MFA$ , and consequently, in specific  
 549 modulus (Fig. 14), with a large range overlap for TW and a small one for CW (Brémaud et al  
 550 2013, Ruelle et al 2007). But no significant relationship was found between  $\alpha_m$  and  $SMB$  (Fig.  
 551 17) although both have large variations. Many papers have described a very significant  
 552 relationship between  $MFA$  and  $\alpha_m$  but they combine NW and RW and the significance comes  
 553 from the RW (Yamamoto et al 1991, Okuyama et al 1994, Yamamoto et al 1998).

554 For CW there is a strong relationship between  $\alpha_m$  and  $SMB$ ; this is similar to all results from  
 555 the literature and is consistent with models built on the assumption of a bulk shrinkage of cell  
 556 wall matrix (Alméras et al 2005a, Yamamoto et al 1988, Guitard et al 1999). The models cannot  
 557 be well adjusted to both NW and CW.

558 For TW although it is admitted that  $MFA$  is always small or very small, the specific modulus is  
 559 not as high as for NW with low  $MFA$ . A tiny tendency of lower  $SM_b$  for higher maturation strain  
 560 (in absolute value) seems to appear for G-layer TW.  $MFA$  cannot explain the high maturation  
 561 strain of TW, and there is no clear difference between G-layer, lignified G-layer and no G-layer  
 562 types of TW regarding the relationship between  $SMB$  and  $\alpha_m$ .

563 One clear indication within each tree is the much higher  $LS$  for both RWs as compared to the  
 564 NW in the same tree (Table 5). But this difference is higher in the case of G-layer TW.

565

Table 5 Differences between normal and reaction wood

Type	$\alpha_m$ NW	$\alpha_m$ RW	RW/NW	LS NW	LS RW	RW/NW	SMB NW	SMB RW	RW/NW
SW	386	<b>-2103</b>	<b>-5.4</b>	0.15	<b>2.10</b>	<b>14.4</b>	21.08	<b>9.01</b>	<b>0.43</b>
HW GL	796	<b>2255</b>	<b>2.8</b>	0.17	<b>0.89</b>	<b>5.3</b>	25.48	<b>28.42</b>	<b>1.12</b>
HW GLc	522	<b>3579</b>	<b>6.9</b>	0.15	<b>1.22</b>	<b>7.9</b>	19.16	<b>24.58</b>	<b>1.28</b>
HW LGL	668	<b>2174</b>	<b>3.3</b>	0.17	<b>0.53</b>	<b>3.0</b>	22.95	<b>29.21</b>	<b>1.27</b>
HW NGL	637	<b>1995</b>	<b>3.1</b>	0.11	<b>0.31</b>	<b>2.9</b>	27.89	<b>32.18</b>	<b>1.15</b>

566

567 SW: Softwood; HW: hardwood; NW: normal wood; RW: reaction wood

567

568 GL: gelatinous layer; GLc: multi-layered GL; LGL: lignified GL; NGL: no GL

568

569  $\alpha_m$ : maturation strain;  $LS$ : longitudinal shrinkage;  $SMB$ : basic specific modulus

569

570 RW/NW: ratio between RW and NW values

570



571 For conifers, the difference of dependence between  $LS$  and  $SM$  for NW and RW was described  
572 before (Watanabe & Norimoto 1996).

573 Models for longitudinal shrinkage of wood (Cave 1972, Yamamoto et al 2001) predict a steady  
574 growth of  $LS$  with growing  $MFA$  over  $30^\circ$  and suggest a small inverse situation for small  $MFA$   
575 below  $30^\circ$ . Remembering that specific modulus is strongly decreasing (from 30 to 10  $Mm^2/s^2$ )  
576 when  $MFA$  increases from 10 to  $30^\circ$  (Cowdrey & Preston 1966, Cave & Hutt 1968, Brémaud et  
577 al 2013),  $LS$  should increase when  $SM_b$  increases in the range 11 to 33  $Mm^2/s^2$  (using the  
578 conversion factor 1.1 between dry specific modulus and  $SM_b$ ). In fact, there was a very  
579 significant negative correlation between  $LS$  and  $SM_b$  for NW in that range. The same seems to  
580 be true also for TW, but  $SM_b$  was supposed to be higher for the low  $MFA$  values in TW.  
581 Moreover, G-layer TW has a much higher  $LS$  than NW for similar values of  $SM_b$ .

582 The paradoxical situation of longitudinal shrinkage for G-layer tension wood was described in  
583 the literature (Dadswell & Wardrop 1955, Jourez et al 2003, Clair & Thibaut 2014). Many  
584 recent papers discuss the role of cellulose nano-fibres organisation within the microfibrils,  
585 using both experiments and models (Clair et al 2008, Chang et al 2015, Alméras & Clair 2016,  
586 Gorshkova et al 2018).  $\alpha_m$  and  $LS$  are considered but these models and could be also efficient  
587 to predict the specific modulus “anomaly” for G-fibres.

#### 588 *Trade-off between active posture control and passive pre-stressing*

589 The tensile pre-stressing of stem periphery enhances its flexure resistance, thanks to the  
590 resistance in tension of wood being typically twice that in compression (Gordon 1978, Thibaut  
591 & Gril 2003, Moulia et al 2006). In order to roughly quantify this, the relationship between  
592 resistance to compression ( $CR$ ) and basic density ( $BD$ ) was examined on the data for green  
593 wood in the wood handbook (Kretschmann 2010).  $CR$  can be predicted by a proportional  
594 formula:  $CR = k \cdot BD$ , where  $k = 52.5$  for softwoods and 46.1 for hardwoods with  $CR$  in MPa and  
595  $BD$  in  $kg/dm^3$ . The specific resistance to compression (resistance/density) is rather unaffected  
596 by microfibril angle (Gindl 2001, Gindl & Teischinger 2002), specifically for CW (Pillow &  
597 Luxford 1937, Cockrell & Knudson 1973), and the same ratio can be used for CW and NW.

598 The same database gives also values of green flexure resistance ( $MOR$ ), roughly twice  $CR$ , that  
599 can be used as a conservative value for tensile strength (Kretschmann 2010); green wood  $MOR$   
600 also can be predicted by a proportional formula:  $MOR = k \cdot BD$ , where  $k = 108$  for both  
601 softwoods and hardwoods. According to a smaller database (18 species), associated to the  
602 large wood handbook database, the green ultimate tensile resistance is in average 60% higher  
603 than green  $MOR$  for the same species (Markwardt & Wilson 1935). Published data of green  
604 TW resistance are scarce. Clarke (1937) writes that tensile strength of TW is 10% higher than  
605 that of NW for beech, while compression strength of TW is much lower, which is consistent  
606 with the higher proportion of cellulose microfibrils in TW. It can also be accepted that green  
607 tensile strength of TW is around 60% higher than its green  $MOR$ .

608 The crude approximation of  $CR$  and  $MOR$  in the green state, based on  $BD$ , was used for all  
609 tested rods. Table 6 summarizes, for NW, TW and CW, the mean values of  $BD$ ,  $CR$  and  $MOR$ ,  
610 together with the maturation stress  $\sigma_m$ . According to the pre-stressing represented by  $\sigma_m$ , in  
611 case of tree bending the maximum allowable compressive stress case is equal to the sum of  
612  $CR$  and  $\sigma_m$ , while the maximum allowable tensile stress is the difference between  $MOR$  and  
613  $\sigma_m$ .

614

Table 6 Pre-stressing and flexure resistance for different wood types

Tree	BD	DPrel	Eg	CR	MOR	$\sigma_m$	$\sigma_m + CR$	MOR- $\sigma_m$
mean CW	0.56	1.26	5.1	29.5	60.8	-9.3	<b>20.2</b>	70.1
mean NW SW	0.46	0.91	10.9	22.4	46.3	3.8	26.2	42.5
mean NW HW	0.47	0.93	11.4	21.7	50.9	8.1	29.7	42.8
mean TW	0.51	1.16	14.4	23.3	54.8	34.3	57.6	<b>20.5</b>

*BD*: basic density (Kg/dm<sup>3</sup>); *Eg*: green modulus of elasticity (GPa);

*DPrel*: ratio between rod distance to pith (*DP*) and mean *DP* for the 8 rods of the tree;

*CR*: longitudinal crushing resistance (MPa); *MOR*: flexure resistance (MPa)

CW: compression wood; NW SW: normal wood of softwood; NW HW normal wood of hardwood;

$\sigma_m$ : maturation stress or pre-stress (MPa)

615  
616  
617  
618  
619  
620

621 For a well-balanced tree containing no RW,  $\sigma_m$  is always positive (tension) on both sides of the  
622 trunk under wind action, and the wind stress  $\sigma$  is maximum and the same in absolute value, on  
623 the two faces: compression downwind, tension upwind. If the maximum wind stress is around  
624 25 MPa for the mean trees of Table 6, the NW will be safe in all wind situations. But for both  
625 types of RW the allowable resistance to compression (case of CW) or to tension (case of TW)  
626 are similar and lower than a wind stress of 25MPa. Stresses due to strong reacting forces may  
627 bring danger in case of wind action either on the compressed side for softwoods or the tensile  
628 side for hardwoods.

629 As *MOR* is likely to be much lower than tensile strength, the situation may not be critical for a  
630 TW side, but for the higher tensile stresses there may be a small wind stress attenuation by  
631 ovalisation of the cross section inducing a growth of the second moment of inertia in the wind  
632 direction.

633 The compressive stress produced by CW is obviously dangerous in case of strong wind  
634 opposite to the CW side. The trade-off between pre-stressing of the skeleton and high force  
635 asymmetry for verticality restoration is managed in a rather sophisticated way as can be  
636 examined on Fig. 11 and Table 6. For CW, density is higher, MOE is much lower and ring width  
637 is much higher - with ovalisation of the cross section. A high compressive force in the newly  
638 formed CW is achieved, despite the very low MOE, by higher density and much higher ring  
639 width. *CR* is higher due to higher density and maturation compressive stress is limited by the  
640 small value of MOE so that the maximum allowable compression stress is not so low.  
641 Moreover, there is a large heterogeneity of MOE within the cross section between CW zone  
642 and the rest. The neutral axis in bending under wind action will no more be in the geometric  
643 centre of the section. As a result, the strain level at periphery will be 15 to 20% higher in the  
644 low modulus portion (the compression wood side) and lower in the other side. As MOE is  
645 much lower in the CW side (2 times lower), the compressive wind stress will be lower than  
646 expected for a normal tree. Ovalisation of the cross section will bring a small additive security  
647 factor and the sum of these compensations should be enough for wind safety in such a case.

## 648 Conclusion

649 The combined growth stress evaluation on standing trees and laboratory measurements of  
650 wood properties on a large range of situations (different species and densities, NW and RW)  
651 bring useful tools for this kind of studies. 1- very good proportional relationships were  
652 established for the relationship between green and dry state for density, specific modulus,

653 longitudinal elastic (MOE) and shearing modulus of elasticity ( $G_{TL}$  and  $G_{RL}$ ). Hence dry wood  
654 properties can be used whether there are no green wood data. 2 - a simple conversion  
655 coefficient ( $\phi$ ) was obtained between growth stress indicator ( $GSI$ ) coming from the single hole  
656 method and maturation strain using the basic specific modulus (ratio between green MOE and  
657 basic density  $BD$ ) and even maturation stress using only basic density for hardwood or  
658 softwood normal wood. The proportionality is true within a tree in all cases, hence  $GSI$  can be  
659 directly used for biomechanical studies at tree level.

660 Basic specific modulus ( $SM_b$ ) and longitudinal shrinkage ( $LS$ ) as well as maturation strain ( $\alpha_m$ )  
661 are properties of cell wall material in the longitudinal direction depending only on the last  
662 fibre living phase (maturation phase, i.e. secondary wall deposition). Microfibril angle ( $MFA$ )  
663 in the secondary wall and chemical composition of cell wall polymers are the underlying  
664 parameters explaining the variations of these 3 properties.  $\alpha_m$  provides a continuum of wood  
665 types from CW to TW through NW, but the analysis of  $SM_b$  and  $LS$  proves that RW cannot be  
666 considered as extreme case of NW but specific patterns as suggested by genomic studies.  
667 Predictive models should be built separately for the 3 types, but the pertinent combined data  
668 on  $\alpha_m$ ,  $MFA$  and chemistry of main polymers is lacking mainly for NW which has an important  
669 contribution to muscular function of the living wood, even in posture regulation. For CW (Yeh  
670 et al 2005) and for non G-layer TW (Baillères et al 1995) the relative composition in lignin  
671 monomers (H/G for softwoods, S/G for hardwoods) was a good predictor of RW. These  
672 parameters can be active also within NW without too much changes in lignin content.

673 By creating forces, the living wood generates tensile residual stresses within the internal  
674 skeleton, improving its resistance to flexure forces as wind action on the compressive side  
675 where the resistance to compression is lower. But high compression pre-stressing on one side  
676 or very high tension pre-stressing on the other side by RW will bring dangerous situations in  
677 case of strong wind in the axis of RW. There is a necessary trade-off between efficient posture  
678 control (by forces) and efficient pre-stressing (by stresses) and compression wood solution  
679 (the most dangerous under wind action) is managed by a complex simultaneous regulation of  
680 strain, modulus of elasticity (via the  $MFA$ ), stress (via the density), force (via the ring width)  
681 and global geometry (via the anisotropy of second moment of area of the section).

## 682 **References**

683 **Alméras T, Thibaut A, Gril J.** 2005b. Effect of circumferential heterogeneity of wood  
684 maturation strain, modulus of elasticity and radial growth on the regulation of stem  
685 orientation in trees. *Trees Structure and function* 19 (4), 457–467. *Trees Structure and*  
686 *function*

687 **Alméras T, Derycke M, Jaouen G, Beauchêne J, Fournier M.** 2009. Functional diversity in  
688 gravitropic reaction among tropical seedlings in relation to ecological and developmental  
689 traits. *Journal of Experimental Botany* 60, 4397–4410.

690 **Alméras T, Clair B.** 2016. Critical review on the mechanisms of maturation stress generation  
691 in trees. *Journal of The Royal Society Interface* 13(122) , 20160550

692 **Alméras T., Jullien D., Gril G.** 2018. Modelling, Evaluation and Biomechanical Consequences  
693 of Growth Stress Profiles Inside Tree Stems. Anja Geitmann, Joseph Gril. *Plant Biomechanics.*  
694 *From Structure to Function at Multiple Scales*, Springer International Publishing, pp.21-48

- 695 **Archer RR.** 1984. Application of a new method for the growth stress measurement for Pinus  
696 Caribea. IUFRO P5-01, Properties and utilisation of tropical woods, Manaus, Brasil, 19 –  
697 23/11/1984
- 698 **Baillères H.** 1994. Précontraintes de Croissance et Propriétés Mécanophysiques de Clones  
699 d'Eucalyptus (Pointe Noire–Congo): Hétérogénéités, Corrélations et Interprétations  
700 Histologiques. Thèse Université Bordeaux I, 162 p
- 701 **Baillères H., Chanson B., Fournier M., Tollier MT., Monties B.** 1995. Structure, composition  
702 chimique et retraits de maturation du bois chez les clones d'Eucalyptus. Annales des sciences  
703 forestières, 52 (2) 157-172.
- 704 **Bordonné P.A.** 1989. Module dynamique et frottement intérieur dans le bois: mesures sur  
705 poutres flottantes en vibrations naturelles. Thèse de Doctorat en Sciences du Bois, Institut  
706 National Polytechnique de Lorraine.
- 707 **Brancheriau L., Baillères H.** 2002. Natural vibration analysis of clear wooden beams: a  
708 theoretical review. Wood Science and Technology (36), 347-365
- 709 **Brémaud I, Ruelle J, Thibaut A, Thibaut B.** 2013. Changes in vibrational properties between  
710 compression and normal wood, roles of microfibril angle and of lignin. Holzforschung 67, 75–  
711 85
- 712 **Brennan M, McLean JP, Altaner CM, Ralph J, Harris PJ.** 2012. Cellulose microfibril angles and  
713 cell-wall polymers in different wood types of Pinus radiata. Cellulose 19, 1385–1404
- 714 **Cave ID.** 1972. A theory of the shrinkage of wood. Wood Science and Technology (6), 284-292
- 715 **Cave ID., Hutt L.** 1968. Anisotropic elasticity of plant cell wall. Wood Science & Technology  
716 2:268–278
- 717 **Clarke SH.** 1937. The distribution, structure and properties of tension wood in beech (*Fagus*  
718 *sylvatica* L.). Forestry 11(2): 85-91
- 719 **Clair B, Ruelle J, Beauchêne J, Prévost MF, Fournier M.** 2006. Tension wood and opposite  
720 wood in 21 tropical rain forest species. 1. Occurrence and efficiency of the G-layer. IAWA  
721 Journal 27 (3), 329–338
- 722 **Clair B, Alteyrac J, Gronvold A Espejo J, Chanson B, Alméras T.** 2013. Patterns of longitudinal  
723 and tangential maturation stresses in Eucalyptus nitens plantation trees. Annals of forest  
724 science 70, 801–811
- 725 **Clair B., Thibaut B.** 2014. Chapter 6 Physical and Mechanical Properties of Reaction Wood. B.  
726 Gardiner et al. eds. The Biology of Reaction Wood, Springer Series in Wood Science, DOI  
727 10.1007/978-3-642-10814-3\_3
- 728 **Cockrell RA., Knudson RM.** 1973. A comparison of static bending, compression and tension  
729 parallel to grain and toughness properties of compression wood and normal wood of a Giant  
730 Sequoia. Wood Science and Technology 7, 241–250
- 731 **Côté WA, Day AC, Timell TE.** 1969. A contribution to the ultrastructure of tension wood fibres.  
732 Wood Science and Technology 3, 257–271

733 **Coutand C, Fournier M, Moulia B.** 2007. Gravitropic response of polar trunk: key roles of the  
734 regulation of wood restressing and of relative kinetics of cambial growth versus wood  
735 maturation. *Plant Physiology* 144, 1166–1180.

736 **Cowdrey DR., Preston RD.** 1966 Elasticity and microfibrillar angle in wood of Sitka spruce. *Proc*  
737 *Roy Soc B* 166:245–272

738 **Cuny HE, Rathgeber CBK, Lebourgeois F, Fortin M, Fournier M,** 2012. Life strategies in intra-  
739 annual dynamics of wood formation: example of three conifer species in a temperate forest  
740 in north-east France. *Tree Physiology* 32, 612–625.

741 **Dadswell HE, Wardrop AB.** 1955. The structure and properties of tension wood.  
742 *Holzforschung* 9, 97–103

743 **Deleuze C., Houllier F.** 1997. A transport model for tree ring width. *Silva Fennica* 31 (3): 239-  
744 250.

745 **Fagerstedt KV, Mellerowicz E, Gorshkova T, Ruel K, Joseleau JP.** 2014. Chapter 3 Cell Wall  
746 Polymers in Reaction Wood. B. Gardiner et al. eds. *The Biology of Reaction Wood*, Springer  
747 Series in Wood Science, DOI 10.1007/978-3-642-10814-3\_3

748 **Fang CH, Clair B, Gril J, Liu SQ.** 2008. Growth stresses are highly controlled by the amount of  
749 G-layer in poplar tension wood. *IAWA Journal* 29 (3), 237–246

750 **Fourcaud T., Zhang X., Stokes A., Lambers H., Körner C.** 2008. Plant Growth Modelling and  
751 Applications: The Increasing Importance of Plant Architecture in Growth Models. *Annals of*  
752 *Botany* 101: 1053–1063, 2008

753

754 **Fournier M, Chanson B, Thibaut B, Guitard D.** 1994b. Measurements of residual growth  
755 strains at the stem surface observations on different species. *Annals of forest science* 51, 249–  
756 266

757 **Fournier M, Bailleres H, Chanson B.** 1994a. Tree biomechanics, growth, cumulative  
758 prestresses, and reorientations. *Biomimetics* 2, 229–251

759 **Fournier M, Alméras T, Clair B, Gril J.** 2014. Chapter 5 Biomechanical action and biological  
760 functions. *The biology of reaction wood.* eds B Gardiner, J Barnett, P Saranpää, J Gril , pp.  
761 139–170. Berlin, Germany, Springer.

762 **Funda T., Fundova I., Gorzsás A., Fries A., Wu HX.** 2020. Predicting the chemical  
763 composition of juvenile and mature woods in Scots pine (*Pinus sylvestris* L.) using FTIR  
764 spectroscopy. *Wood Science and Technology* 54:289–311

765 **Gardiner B, Barnett J, Saranpää P, Gril J.** 2014. *The biology of reaction wood.* Springer, Berlin,  
766 Heidelberg

767 **Gibson L.J., Ashby M.F.** 1999. *Cellular Solids: Structure and Properties*, Cambridge University  
768 Press, 2nd edition.

769 **Ghislain B., Engel J., Clair B.** 2019. Diversity of anatomical structure of tension wood among  
770 242 tropical tree species. *IAWA journal.* 40(4) 765-784

771 **Gindl W.** (2001) The effect of lignin on the moisture-dependent behaviour of spruce wood in  
772 axial compression. *JOURNAL OF MATERIALS SCIENCE LETTERS* 20, 2161 – 2162

773 **Gindl W., Teischinger A.** (2002) Axial compression strength of Norway spruce related to  
774 structural variability and lignin content. *Composites: Part A* 33, 1623–1628

775 **Glass SV, Zelinka SL.** 2010. Chapter 4, Moisture relations and physical properties of wood in  
776 Wood handbook—Wood as an engineering material. General Technical Report FPL-GTR-190.  
777 USDA, Forest Service, Forest Products Laboratory.

778 **Gordon JE.** 1978. Structures, or why things don't fall down. Penguin Books, Harmondsworth

779 **Gorshkova T, Brutch N, Chabbert B, Deyholos M, Hayashi T, Lev-Yadun S, Mellerowicz EJ ,**  
780 **Morvan C, Neutelings G, Pilate G.** 2012. Plant fibre formation, state of the art, recent and  
781 expected progress, and open questions. Critical Review in Plant Sciences 31, 201–228

782 **Gorshkova T, Chernova T, Mokshina N, Ageeva M, Mikshina P.** 2018. Plant “muscles”, fibers  
783 with a tertiary cell wall. New Phytologist 218 (1), 66–72

784 **Gril J., Jullien D., Bardet S., Yamamoto H.** 2017. Tree growth stress and related problems.  
785 Journal of Wood Science, 63 (5), pp. 411-432.

786 **Guitard D., El Amri F.,** Modèles prévisionnels du comportement élastique tridimensionnel  
787 des bois feuillus ou résineux, Annales des Sciences Forestières 44 (1987) 335–358.

788 **Huang YS., Chen SS., Lin TP., Chen YS.** 2001. Growth stress distribution in leaning trunks  
789 of *Cryptomeria japonica*. Tree Physiology 21, 261–266

790 **Jourez B., Riboux A., Leclercq A.** 2001a. Comparison of basic density and longitudinal  
791 shrinkage in tension wood and opposite wood in young stems of *Populus euramericana* cv.  
792 Ghoy when subjected to a gravitational stimulus. Canadian journal of forest research  
793 31(10):1676-1683

794 **Jourez B., Riboux A., Leclercq A.** 2001b. Anatomical characteristics of tension wood and  
795 opposite wood in young inclined stems of poplar (*Populus euramericana* CV 'Ghoy'). IAWA J.  
796 22: 133–157.

797 **Jullien D, Widmann R, Loup C, Thibaut B.** 2013. Relationship between tree morphology and  
798 growth stress in mature European beech stands. Annals of forest science 70 (2), 133–142

799 **Kretschmann DE.** 2010. Chapter 5, Mechanical properties of wood. Wood handbook—Wood  
800 as an engineering material. General Technical Report FPL-GTR-190. USDA, Forest Service,  
801 Forest Products Laboratory.

802 **Leonardon M, Altaner CM, Vihermaa L, Jarvis MC.** 2010. Wood shrinkage, influence of  
803 anatomy, cell wall architecture, chemical composition and cambial age. European journal of  
804 wood and wood products 68, 87-94

805 **Mellerowicz EJ, Baucher M, Sundberg B, Boerjan W.** 2001. Unravelling cell wall formation in  
806 the woody dicot stem. Plant Molecular Biology 47 1-2, 239-274.

807 **Moulija B, Coutand C, Lenne C.** 2006. Posture control and skeletal mechanical acclimation in  
808 terrestrial plants: implications for mechanical modeling of plant architecture. Am. J.

809 **Nanayakkara B., Manley-Harris M., Suckling I.D., Donaldson LA.** 2009. Quantitative chemical  
810 indicators to assess the gradation of compression wood. Holzforschung 63:431 – 439.

811 **Okuyama T., Yamamoto H., Yoshida M., Hattori Y., Archer RR.** 1994. Growth stresses in  
812 tension wood, role of microfibrils and lignification. Annals of forest science 51, 291–300.

813 **Pillow MY., Luxford RF.** (1937) Structure, occurrence and properties of compression wood.  
814 Technical bulletin N° 546, USDA, Washington, 32p.

- 815 **Plomion C, Leprovost G, Stokes A.** 2001. Wood formation in trees. *Plant Physiology* 127 (4),  
816 1513-1523.
- 817 **Ruelle J.** 2014. Chapter 2 Morphology, Anatomy and Ultrastructure of Reaction Wood. B.  
818 Gardiner et al. eds. *The Biology of Reaction Wood*, Springer Series in Wood Science, DOI  
819 10.1007/978-3-642-10814-3\_3
- 820 **Ruelle J, Yamamoto H, Thibaut B.** 2007. Growth stresses and cellulose structural parameters  
821 intension and normal wood from three tropical rainforest angiosperm species. *Bioresources*,  
822 235–251
- 823 **Thibaut B., Gril J., Fournier M.** 2001. Mechanics of wood and trees, some new highlights for  
824 an old story. *Comptes Rendus de l'Académie des Sciences Paris, série II B* 329 (9), 701–716
- 825 **Thibaut B., Gril J.** 2003. Growth stresses. In: Barnett JR, Jeronimidis G (eds) *Wood quality*  
826 and its biological basis. Blackwell, Oxford, pp 137–156
- 827 **Thibaut B.** 2019. Three-dimensional printing, muscles and skeleton: mechanical functions of  
828 living wood, *Journal of Experimental Botany*, Volume 70, Issue 14, 1 July 2019, Pages 3453–  
829 3466
- 830 **Timell TE.** 1986. *Compression wood in gymnosperms*, 3 vol. Springer, Berlin, 2210 pp
- 831 **Trouvé R., Bontemps JD., Seynave I., Collet C., Lebourgeois F.** 2015. Stand density, tree social  
832 status and water stress influence allocation in height and diameter growth of *Quercus petraea*.  
833 *Tree Physiology* 35, 1035–1046
- 834 **Vieilledent G, Fischer FJ, Chave J, Guibal D, Langbour P, Gérard J** (2018). New formula and  
835 conversion factor to compute basic wood density of tree species using a global wood  
836 technology database. *American Journal of Botany* 105(10): 1–9.
- 837 **Watanabe U., Norimoto M.** 1996. Shrinkage and elasticity of normal and compression wood  
838 in conifers. *Mokuzai Gakkaishi* 42 (7), 651-658
- 839 **Yamamoto H., Okuyama T.** 1988. Analysis of the generation process of growth stresses in cell  
840 walls. *Mokuzai Gakkaishi* 34 (10), 788-793
- 841 **Yamamoto H., Okuyama T., Sugiyama K., Yoshida M.** 1991. Generation process of growth  
842 stresses in cell walls III. Growth stress in compression wood. *Mokuzai Gakkaishi* 37 (2), 94-100
- 843 **Yamamoto H., Okuyama T., Yoshida M.** 1998. Growth stress generation and microfibril  
844 angle in reaction wood. In: Butterfield BG (ed) *Microfibril angle in wood*. International  
845 Association of Wood Anatomist, Christchurch, pp 225–239
- 846 **Yamamoto H., Sassus F., Ninomiya M, Gril J.** 2001. A model of anisotropic swelling and  
847 shrinking process of wood. Part 2. A simulation of shrinking wood. *Wood Science and*  
848 *Technology* 35: 167-181
- 849 **Yamashita S., Yoshida M., Takayama S., T. Okuyama T.** 2007. Stem-righting mechanisms in  
850 gymnosperm trees deduced from limitations in compression wood development. *Annals of*  
851 *Botany*. 99 487–493.
- 852 **Yang JL, Baillères H, Okuyama T, Muneri A, Downes G.** 2005. Measurement methods for  
853 longitudinal surface strain in trees, a review. *Australian Forestry* 68, 34–43

- 854 **Yeh TF, Goldfarb B, Chang HM, Peszlen I, Braun JL, Kadla JF.** 2005. Comparison of  
855 morphological and chemical properties between juvenile wood and compression wood of  
856 loblolly pine. *Holzforschung* 59, 669–674
- 857 **Yeh TF, Braun jL, Goldfarb B, Chang HM, Kadla, J.F.** 2006. Morphological and chemical  
858 variations between juvenile wood, mature wood, and compression wood of loblolly pine  
859 (*Pinus taeda* L.). *Holzforschung*. 60, 1-8
- 860 **Yoshida M, Okuda T, Okuyama T.** 2000. Tension wood and growth stress induced by artificial  
861 inclination in *Liriodendron tulipifera* Linn. and *Prunus spachiana* Kitamura f. *ascendens*  
862 Kitamura. *Annals of forest science* 57 (8), 739–746
- 863 **Yoshida M, Okuyama T.** 2002. Techniques for measuring growth stress on the xylem surface  
864 using strain and dial gauges. *Holzforschung* 56 (5), 461–467